DOI: https://doi.org/10.2138/am-2019-6906

Revision – 1

Constraining The Timing and Character of Crustal Melting in the Adirondack Mountains Using Multiscale Compositional Mapping and In-Situ Monazite Geochronology

Michael L. Williams[1], Timothy Grover[2], Michael J. Jercinovic[1], Sean P. Regan[3], Claire R. Pless[1], and Kaitlyn A. Suarez[1]

1 – Department of Geosciences, University of Massachusetts, Amherst, MA 01003, mlw@umass.edu.

2 – Department of Earth and Atmospheric Sciences, University of Northern Colorado, Greeley, CO 80639

3 – Department of Geosciences, University of Alaska Fairbanks, Fairbanks, AK 99775

Abstract

Migmatites are common in the hinterland of orogenic belts. The timing and mechanism (in-situ vs external, P-T conditions, reactions, etc.) of melting are important for understanding crustal rheology, tectonic history, and orogenic processes. The Adirondack Highlands have been used as an analog for mid/deep crustal continental collisional tectonism. Migmatites are abundant, and previous workers have interpreted melting during several different events, but questions remain about the timing, tectonic setting, and even the number of melting events. We use multiscale compositional mapping combined with in-situ geochronology and geochemistry of monazite to constrain the nature, timing, and character of melting reaction(s) in one locality from the eastern Adirondack Highlands. Three gray migmatitic gneisses, studied here, come from close proximity and are very similar in microscopic and macroscopic (outcrop) appearance. Each of the rocks is interpreted to have undergone biotite dehydration melting (i.e. Bt + Pl + Als + Qtz = Grt + Kfs + melt). Full-section compositional maps show the location of reactants and products of the melting reaction, especially prograde and retrograde biotite, peritectic K-feldspar, and leucosome, in addition to all monazite and zircon in context. In addition, the maps provide

DOI: https://doi.org/10.2138/am-2019-6906

constraints on kinematics during melting and a context for interpretation of accessory phase composition and geochronology. More so than zircon, monazite serves as a monitor of melting and melt loss. The growth of garnet during melting leaves monazite depleted in Y and HREEs while melt loss from the system leaves monazite depleted in U. Results show that in all three localities, partial melting occurred during at ca. 1160-1150 Ma (Shawinigan orogeny), but the samples show high variability in the location and degree of removal of the melt phase, from near complete, to dispersed, to segregated into leucosomal layers.". All three localities experienced a second high-T event at ca. 1050 Ma, but only the third (non-segregated) sample experienced further melting. Thus, in addition to bulk composition, the fertility for melting is an important function of the previous history and the degree of mobility of earlier melt and fluids. Monazite is also a sensitive monitor of retrogression; garnet breakdown leads to increased Y and HREE in monazite. Results here suggest that all three samples remained at depth between the two melting events but were rapidly exhumed after the second event.

Keywords

Monazite petrochronology, migmatite, polymetamorphism, Adirondack Highlands

Introduction

Metamorphic terranes with evidence for high or even ultra-high temperature metamorphism have been increasingly recognized in orogenic belts around the world (Kelsey and Hand, 2015; Korhonen et al., 2014). Many of these regions involve significant partial melting, which in turn, has important implications for changing rheology, strain localization, petrogenesis of derived igneous rocks, and for interpretations of tectonic history and tectonic processes in general. In order to constrain the conditions of metamorphism as well as the composition of melts, the degree of partial melting, and the degree to which melt has been lost from the system, it is particularly important to characterize the conditions of melting and the dominant melting reaction(s). Fortunately, new geothermometers, thermodynamic databases, and phase equilibria modeling techniques are increasingly able to accommodate high temperatures, and partial melting, allowing many new insights into the tectonics of migmatitic rocks (White and Powell, 2002; White et al., 2007; Dumond et al., 2015; Koblinger and Pattison, 2017). One common question, critical for interpreting the tectonic setting of high-T metamorphism, concerns the timing of melting. Timing constraints typically come from isotopic dating of high-T minerals such a zircon or monazite. Especially in multiply deformed and/or multiply metamorphosed regions, geochronologic analysis requires in-situ dating after careful textural analysis to identify domains that represent particular melting/crystallization events.

The Adirondack Mountains of New York are a classic example of a high-grade, polydeformational terrane that has been used as an analog for middle to deep crustal continental collisional and extensional tectonism (Mezger, 1992; Selleck et al., 2005; Rivers, 2008). Numerous studies have been done to characterize the nature and grade of metamorphism and deformation (Bohlen et al., 1985; Spear and Markussen, 1997; Storm and Spear, 2005). Many rocks show evidence for significant degrees of partial melting, and it is likely that, at least in some rocks, significant amounts of melt have been lost from the local system. Previous workers have interpreted melting during one (or several) orogenic or thermal/magmatic events, but in many regions, questions remain about the timing, tectonic setting, and even the number of partial melting events. In order to interpret the tectonic history of the region and use the region as an analog for modern deep crust, it is critical to constrain the timing, setting, and rheologic implications of melting.

Multiscale compositional mapping combined with high-spatial-resolution (micron-scale), in-situ geochronology and geochemistry of monazite can provide significant insight into the nature of melting reaction(s), the timing of melting, the relationship to deformational events, and the ultimate significance of companion zircon geochronology (Williams et al., 2017). In this paper, we apply this technique to several samples from a migmatite locality in the eastern Adirondack Mountains. The results suggest that melting occurred primarily near the end of the Shawinigan orogeny and during the regional (1155 Ma) Anorthosite - Mangerite- Charnockite-Granite (AMCG) magmatic event, but different samples preserve dramatically different melting and melt loss histories. Further, at least in some rocks, a biotite dehydration melting reaction went to near completion, and little of the melt component remains in the rock. Other rocks retained a larger proportion of the melt component and these were susceptible to a second stage of melting, approximately 100 m.y. later. It will be necessary to apply these techniques more generally in order to build a comprehensive model for melting in the Adirondack Mountains, but the results presented here have a number of implications for the tectonic history of the region and for the rheology of the deep crust in general. Our results provide a template for future studies in this region and in other regions in order to compare and interpret the tectonic setting of migmatitic rocks.

Geologic Background

Mesoproterozoic rocks of the Adirondack Mountains formed during a series of accretionary/collisional orogenic events generally referred to as the Grenville Orogenic cycle (Rivers, 2008; Chiarenzelli et al., 2010; McLelland et al., 2013). The region has been divided into the Adirondack Lowlands and Highlands (Fig. 1), separated by the Carthage-Colton shear zone (Selleck et al., 2005). Most workers now recognize several major stages in the overall tectonic history, although not all of these events have been recognized in the Adirondacks. The ca. (1245-1220 Ma) Elzevirian orogeny is interpreted to represent a period of arc and back-arc accretion on or near the margin of Laurentia (McLelland et al., 2013). The (ca.1190-1140 Ma) Shawinigan orogeny is interpreted to represent a period of accretionary orogenesis possibly during back arc collapse, collision with a >1.3 Ga tonalitic arc, and finally, left-lateral transpression (Chiarenzelli et al., 2010). The effects of this orogenic event have been increasingly recognized in the Adirondack Highlands in recent years (Chiarenzelli et al., 2011a). The voluminous (ca. 1155Ma) AMGC magmatic event involved gabbro, anorthosite, mangerite, charnockite, and granite, which were emplaced at the very end of the Shawinigan Orogeny and interpreted to be a result of lithospheric delamination (McLelland et al., 2004; Regan et al., 2011). The 3000 km^2 Marcy anorthosite massif (1154 +/- 6 Ma; McLelland et al. 2004; Hamilton et al. 2004), a member of this suite, is the dominant plutonic body in the Adirondack Highlands (Buddington, 1939).

The (ca. 1090-1020 Ma) Ottawan orogeny has traditionally been considered to have been a major continent-continent collision, involving large-scale thrusting and folding in the Adirondack Highlands (McLelland et al., 1996, 2001). Recently, however, at least the later part of the orogeny (ca. 1070-1030) has been interpreted as an extensional event with localized normal shearing on the Highlands-bounding, Carthage Colton and East Adirondack shear zones (Selleck et al., 2005; Wong et al., 2012; Regan et al., 2019). The latest events in the cycle involved pegmatite emplacement, metasomatism, and local (ca. 980 Ma) disturbance (Lupulescu et al. 2011). Tectonism in this age range has been termed the Rigolet stage or orogeny (Rivers, 2008), a significant event in the western Grenville Province but one that is interpreted to have had a minimal impact on the structural and metamorphic architecture in the Adirondack region.

In addition to plutonic rocks, the Adirondack Highlands region contains abundant garnet-rich migmatitic gneisses, interpreted to have been derived from Al-rich sedimentary protoliths (Storm and Spear, 2005). Although leucosome layers, veins, and pods are common, many rocks are dominated by garnet (10s of percent), sillimanite, quartz, and feldspar, with variable amounts of prograde and retrograde biotite. Many of the, biotite-poor, sillimanite-rich rocks have been termed “khondalite” (McLelland et al., 2002), and have been interpreted to be residues (restites), having lost some component of partial melt.

Bickford et al. (2008) and Heumann et al. (2006) carried out U-Pb zircon (IDTIMS) analyses, and Heumann combined in-situ monazite dating, in order to constrain the timing and setting of melting in the Adirondack Highlands and Lowlands. Heumann et al. (2006) concluded that melting occurred primarily during the Shawinigan orogeny, which was cited as 1210-1160 Ma and also during AMCG magmatism, cited as 1165-1150 Ma. Bickford et al. (2008) investigated additional localities and concurred that melting occurred in many regions during the Shawinigan and AMGC events, but they also found evidence for melting at ca. 1050 Ma (Ottawan), particularly in the eastern Adirondack Highlands. They suggested that Ottawan metamorphic temperatures were probably high, but melting occurred only locally due to fluid influx or local decompression melting of the dry generally residual rocks.

Samples investigated in this study came from roadcuts along Route-8 in the eastern Adirondack Mountains. The three specific localities chosen, here called the Swede Mountain, Treadway Mountain, and Elephant Rock areas (Fig. 1), were selected because of the presence of large, relatively fresh roadcut exposures of garnet-rich migmatitic rocks. These localities have been common field trip stops in recent years, and in addition, Bickford et al. (2008) concluded that melting at the Treadway Mtn. locality occurred during the Ottawan, possibly in addition to the earlier Shawinigan orogeny. These potentially-multistage migmatitic rocks appear to be particularly appropriate targets for in-situ monazite dating (i.e. “reaction dating”, Williams et al., 2017), in order to evaluate the degree to which monazite analysis can provide insight into the melting (and tectonic) history of the region.

Methods

The general approach to *in-situ* monazite dating is summarized in Williams et al. (2006) and updated in Williams et al. (2017). The workflow involves selection of samples based on assemblage, deformational characteristics, tectonic setting etc. Full-section compositional maps are collected early in the analytical process using the Cameca SX50 electron microprobe at the University of Massachusetts. For this study, maps were collected for Mg, K, Ca, Ce, and Zr. The Mg, K, and Ca maps show the distribution of the major silicate phases. Ce and Zr maps show the location of all monazite and zircon grains respectively (See Williams et al., 2006). The full-section maps also allow quick calculation of modes of all major and minor phases.

High resolution maps are then collected for a number (typically 20 or more) monazite grains in the section. Maps for Y, Th, U, Ca, and one other element (Si, Nd, Gd, As, etc.) are collected. The maps are processed simultaneously such that intensities are comparable from grain map to grain map (Williams et al., 2006; 2017). It is particularly informative for high-resolution maps to be placed around the full-section image with links to the actual grain locations (see below). This allows the zonation within a high-resolution map to be interpreted in the context of its textural and microstructural setting within the thin section. Important domain types are selected from the combined assemblage of grain maps; commonly between 3 and 6 domain types are present in a typical thin section. Typically, a “domain” is a compositionally homogeneous region in one or more monazite grains. Some domains are defined by their textural setting in the thin section (i.e. inclusions in garnet, alignment with fabric, etc.). Finally, a dating strategy is developed whereby each domain type is sampled (dated) several times with preference given to grains where two or more domains can be sampled from the same grain.

Monazite dating was carried out on the Cameca Ultrachron electron microprobe at the University of Massachusetts. The instrument was specifically designed for trace-element analysis and dating (Jercinovic et al., 2008). The analytical protocol is described in Williams et al. (2017), and is briefly summarized here. For each compositionally-defined domain, a single background analysis is acquired first, followed by 6-8 peak measurements near the background location. Background intensities are determined using the "multipoint" method (Allaz et al., 2019); measurements are made in four to eight locations on either side of the peak position. The bremsstrahlung curve is determined by (Savitzky-Golay) regression of acceptable measurements, and then the background is calculated at the peak position. One "date" is calculated for each domain. Uncertainty is calculated by propagating measurement and background errors through the age equation (Williams et al., 2006). Typically, dates are shown as a single Gaussian probability distribution function (curve) for the dated domain.

Although metamorphic temperatures were relatively high (ca. 800 °C), there is essentially no evidence of U, Th, or Pb diffusion or of resetting of dates. Compositional maps show straight sharp domain boundaries. Multiple analyses within the same compositional domain, regardless of size, yield no systematic variation toward grain edges or domain boundaries, and MSWD values suggest that variation from point to point primarily reflects electron beam counting statistics. We suggest that, even at these temperatures, diffusion of U, Th, and Pb is too slow to significantly affect the calculated dates. This is consistent with the conclusions of Cherniak et al. (2004) who suggested closure temperatures of ca. 900 °C even for relatively small (10 μm) monazite grains. However, compositions and dates can be modified at lower temperature by alteration processes such as dissolution-reprecipitation, but these processes are typically apparent from textural and compositional characteristics (Williams et al., 2011; 2017).

Results

Petrography

Samples were collected from outcrops along Rt. 8 near Hague, NY. Five samples from three localities are of particular interest here. Samples 16TG-151a and b were collected from the Treadway Mountain area (also locality 9 from Bickford et al., 2008); samples 16TG-153 and154 were collected from the area of Swede Mountain locality described by McLelland et al., 2002); and sample 16TG-150 was collected further east at a locality locally known as Elephant Rock (Fig.1). 16TG-154 (Swede Mtn.) is the main sample from which data will be summarized here, although data from the other samples will be used to provide additional constraints and insight. All of the samples are interpreted to be paragneisses, aluminous metasedimentary rocks. Sample 16TG-153 was an aluminous (impure?) quartzite; the other samples were probably pelitic in composition.

All of the samples are similar in mineralogy and general appearance in outcrop and thin section (Fig. 2). They are layered garnet-rich grey migmatitic gneisses with leucosome layers that vary from millimeters to centimeters in thickness. Gray non-leucosome layers contain sillimanite, biotite, lavender-colored garnet, feldspar, and quartz with accessory monazite, zircon, ilmenite, and apatite. Although size, shape, and composition of the feldspar varies from sample to sample (see below), in hand sample, feldspars are grey in color without obvious striations or twining. It can be very difficult, in hand specimen or even thin section, to estimate the relative proportion of alkali and plagioclase feldspar.

Garnet crystals range from several millimeters to more than 1cm in diameter. They are typically subhedral to augen-shaped. Small garnet fragments commonly occur along the foliation near larger crystals and the geometry suggests that they were fractured and dispersed away from the larger crystals. Many garnet crystals have inclusion–rich cores, commonly Qz, Bt, and Ilm, with inclusion-poor rims (i.e. Fig. 2c). Biotite commonly occurs in strain shadows associated with garnet and to varying degrees, dispersed in the matrix. Matrix biotite is least abundant (trace to 1%) in samples 16TG-154 (Swede Mountain) and 16TG-150 (Elephant Rock) and relatively abundant (5-10%) in 16TG-151 (Treadway Mtn.) (see discussion below). Sillimanite is also abundant (several percent) in samples 150 and 154 and rare, but present, in sample 151.

Gneissic layering is defined by leucocomes layers and by aligned sillimanite, biotite, and, to varying degrees, by dynamically recrystallized feldspar. The fabric dips shallowly (<20°), either east or west, with northerly strike at each locality. Small-scale rootless isoclinal folds of the main foliation/layering are present, typically defined by folded leucosome layers. Some larger-scale isoclinal folds were described by (McLelland et al., 2002), but were not observed in the outcrops sampled here.

Mineral lineations are not particularly apparent in outcrop or hand sample. Based on observation of many outcrops in the eastern Adirondack Mountains, migmatitic (khondalitic) gneiss in general seem to preserve little or no lineation relative to non-migmatitic rocks. We suspect that rocks deforming with a significant melt component may be less likely to form strong lineations (see discussion below). The one exception is 16TG-153 (quartzite), which has a relatively strong lineation (plunging 16° toward 096°) defined by quartz rods, sillimanite, and

DOI: https://doi.org/10.2138/am-2019-6906

elongate biotite books. *All samples were cut parallel to this lineation and perpendicular to gneissic layering/foliation.* If this orientation is representative, then, all of these generally E-W trending outcrops may be appropriate for making kinematic observations.

Leucosomes are dominated by quartz and differing proportions of plagioclase and K-feldspar with minor amounts of biotite. . Lavender to ruby-colored garnet can be present or absent and is distinctly less abundant than in the non-leucosome layers. Oxides are not abundant and consist of ilmenite and locally magnetite. Accessory phases include monazite, zircon, and apatite.

Compositional Mapping

Figure 3 shows full-thin-section compositional maps from the three main metapelitic samples. Major differences occur in the mode, composition and distribution of feldspar and also in the mode and distribution of biotite. These differences tend to be better defined on the compositional maps compared to photomicrographs because individual minerals (or even compositional domains) can be isolated. Sample 16TG-154 contains only K-feldspar (Fig. 3a,b). All other phases in the common assemblage are present, biotite, garnet, quartz, sillimanite, apatite, rutile, zircon, and monazite. The K-feldspar is extremely abundant making up much of the matrix of the sample (Fig. 3b). It occurs in continuous layers wrapping around garnet, forming strain shadows near garnet, and locally occurs as sigma-style porphyroclasts.

Plagioclase is abundant and widely distributed in sample 16TG-151 (Treadway Mtn.) (Fig. 3g, h). The plagioclase is coarser-grained in some layers compared to others, and in some coarser layers, the plagioclase defines sigma-style core-and-mantle structures. Fine grained layers contain small (3-5 mm) dispersed garnet. Coarser-grained layers tend to be garnet-poor although some have discontinuous selvages of relatively coarse garnet. The coarser layers are only slightly lighter colored in hand specimen. They are interpreted to have contained a greater component of partial melt than the finer layers. Sample 16TG-150 contains moderately abundant plagioclase, but unlike 16TG-151, the plagioclase is commonly concentrated near garnet and typically forms σ tails associated with large garnet porphyroblasts or it occurs in layers that seem to have flowed around and away from garnet (Fig. 3d,e). Although some of this plagioclase may result from retrograde consumption of garnet, possibly reversal of the melting reaction, we suggest (below) that some, and perhaps most, of this plagioclase was present in the melt phase and crystallized during deformation in strain shadows near garnet.

Sample 16TG-150 (Elephant Rock) and 16TG-154 (Swede Mountain) have relatively little biotite (Fig. 3c,f), and as noted above, virtually all is located near garnet, especially as moderately foliated sigma tails and "quarter structurers" (Hanmer and Passchier, 1991). Sample 16TG-154 contains several small matrix biotite grains that are distinctly, almost completely, rimmed by small garnet crystals. These are interpreted to be early grains that were not completely consumed during the melting reaction (see below). As noted above, sample TG16-151 (Treadway Mountain) contains abundant dispersed, well foliated biotite (Fig. 3i).

P-T Conditions

The peak mineral assemblage for all of the samples investigated here includes garnet, K-feldspar, quartz, sillimanite, ilmenite +/- biotite, and plagioclase. Much of the biotite and some plagioclase is interpreted to have resulted from melt crystallization or retrograde metamorphism (see below). Phase diagrams have been calculated by a number of workers for pelitic and semi-pelitic bulk compositions, and relationships for moderate-pressure amphibolite/granulite facies rocks are very similar among the various grids (Storm and Spear, 2005; White, et al., 2007; Yakymchuk and Brown, 2014; Yakymchuk, 2017). Assemblages for all of our samples fall within the region shown on Figure 4 (from White et al., 2007), approximately 725-825 ºC and 0.6-0.9 GPa.

Estimates of temperature and pressure are rather uniform, on the scale of many kilometers, across the Adirondack highlands (Bohlen et al., 1985; Spear and Markussen, 1997; Storm and Spear, 2005). Peak conditions have been interpreted to be in the range of 0.7-0.8 GPa, 700-800 °C based on phase relationships (Storm and Spear, 2005) and also on calculations using various geothermometers and geobarometers (Bohlen et al., 1985; Spear and Markussen, 1997; Storm and Spear, 2005; Chiarenzelli et al., 2011b). Temperatures may have varied over the large Adirondack Highlands region to some degree (Bohlen et al., 1985). However, it is unlikely that significant thermal gradients existed on the local scale (~3 km) of our samples. Instead, we suggest that all of the samples experienced similar metamorphic conditions and followed a similar P-T history. This observation/interpretation is discussed below in light of our new monazite results.

Melting Reactions

Phase relationships, particularly the rarity of peak biotite and plagioclase and the abundance of garnet and K-feldspar, suggest that the following were important melting reactions at all three of our sample localities

$$\mathrm{Bt + Pl + Als + Qtz = Grt + Kfs + melt} \qquad (1)$$

$$\mathrm{Bt + Als + Qtz = Grt + Kfs + melt} \qquad (2)$$

Some initial melting may have been associated with muscovite dehydration, but modeling suggests that the amount of melting (i.e. melt production) was probably limited (Storm and Spear, 2005; Yakymchuk and Brown, 2014). The complete lack of plagioclase in sample 16TG-154 (Swede Mountain) suggests that Reaction-1 was exceeded. Several biotite crystals are

This is a preprint, the final version is subject to change, of the American Mineralogist (MSA)
Cite as Authors (Year) Title. American Mineralogist, in press.
DOI: https://doi.org/10.2138/am-2019-6906

surrounded by garnet and are interpreted to relict prograde grains. These may suggest that Reaction-2 was not entirely exceeded, but alternatively the garnet may have shielded the rare prograde biotite. The lack of plagioclase in sample 16TG-154 also indicates that Reaction-1 was not significantly reversed during melt crystallization and retrograde metamorphism. The abundance of K-feldspar and garnet, similarly, suggests that Reaction-2 was not significantly reversed. Sample 16TG-154 does contain biotite, but at least some of this biotite may reflect late biotite growth associated with fluid influx long after melting. Because of the lack of reversal of the melting reactions and the lack of plagioclase- and quartz-bearing leucosome, it seems likely that a portion of the melt component was removed from the local rock, leaving behind a residual bulk composition.

Samples 16TG-151 and 16TG-150 contain both plagioclase and K-feldspar, but have distinctly different textures. 16TG-150 contains coarse grained K-feldspar and plagioclase, particularly in the shadows of large garnet porphyroblasts. Leucosome layers with annealed or undeformed feldspars wrap around the garnet porphyroblasts. Samples from locality151 contain dispersed, fine to medium grained, plagioclase and K-feldspar. Leucosome layers, typically several centimeters thick, are present in the outcrop, but although the sample has plagioclase richer and poorer layers, distinct leucosome layers with sharp boundaries are not present in the analyzed sections.

In summary, our three of our sample localities are likely to have experienced similar metamorphic histories and peak conditions. Although some melt injection is possible, the garnet-rich, restitic assemblages suggest that all samples underwent some partial melting. However, samples 151 and 150 either apparently did not melt to as great an extent or they retained a larger proportion of the melt component. In addition, sample 16TG-150 ended up with a distinctly layered texture while 16TG-151 ended up with a much more homogeneous non-layered texture. The variations may reflect subtle differences in the original bulk composition, but they may also have involved different amounts of strain partitioning that, in turn, helped to facilitate melt segregation/removal (see below).

Monazite Results

We analyzed more than 100 monazite grains from five polished section (2 sections from Treadway Mountain; 2 from Swede Mountain; and 1 section from Elephant Rock). Most of the grains have multiple compositional domains. Monazite from all samples have distinct similarities. Yttrium concentration defines the major domains. High-Y cores are present in approximately one third to one half of the grains in any sample. The cores tend to be small, on the order of 10-20 micrometers in diameter, and anhedral to subhedral. Some cores are surrounded by one or more outer core domains with somewhat lower Y content. These tend to be narrow (5-10µ or less) and irregular. The largest domain in most monazite grains has the lowest Y content. These are the dominant interior domains in grains without cores, and in grains with high-Y cores, they can vary from tens to hundreds of micrometers in thickness. Most monazite grains have narrow higher-Y rim domains. Some rims get as thick as 5-10µ, but most are less than 5µ. For the purpose of the following description and discussion, the major monazite domains will be referred to as from inside outward: 1) core, 2) outer core, 3) main, and 4) rim domains.

Monazite inclusions in garnet are not abundant, but some occur in most samples. The cleanest inclusions, i.e. monomineralic inclusions without cracks in the surrounding garnet, contain high yttrium concentrations comparable to monazite cores (above). Inclusions within fractured garnet can have complex zoning. Typically, parts of the inclusion grains have high Y,

DOI: https://doi.org/10.2138/am-2019-6906

but parts have mottled zoning suggesting alteration by fluids. Inclusion grains are not common enough in these samples to evaluate differences in monazite composition between garnet cores and rims.

Calculated dates will be discussed below in the context of monazite composition. However, in general, dates are very consistent among the five samples. Some high-Y cores yield dates as old as 1250-1225 Ma, but most cores are in the range of 1170-1150 Ma. Outer cores can be either ca. 1150 Ma or more commonly ca. 1060 Ma. The main (low-Y) domains are invariably 1050-1020 Ma and most are ca. 1050 Ma. High-Y rims are typically 1030 Ma and younger. Rim domains with the highest-Y content are invariably younger than 1000 Ma.

Monazite composition-age relationships

Sample 16TG-154 Figure 5a shows calculated monazite dates for sample 16TG-154 (Swede Mountain). As noted, each probability distribution represents one monazite date, obtained from one compositional domain as delineated by grain mapping. A "date" represents one "multipoint" background determination and approximately six peak measurements made immediately adjacent to the background position (see discussion in Williams et al., 2017). The compositional homogeneity of the particular domain is assessed by variability of the peak measurements. Color codes (Fig. 5a) show the main domain types (i.e. core, outer core, main, rim). All calculated dates are included in Supplemental Document X with uncertainty. Typical uncertainties range from ca. 4 m.y. to very rarely greater than 20 m.y (2σ). Uncertainties include short term (random) counting statistics associated with peak and background measurement propagated through the age equation, as well as uncertainty introduced by compositional heterogeneity within the monazite domain (see discussion in Williams et al., 2006; 2017).

This is a preprint, the final version is subject to change, of the American Mineralogist (MSA)
Cite as Authors (Year) Title. American Mineralogist, in press.
DOI: https://doi.org/10.2138/am-2019-6906

Footnote: We use the term "date" to refer to the results of a calculation using the "age equation" of Montel et al., 1996) and the measured U-Th-Pb values. The term "age" refers to the interpretation of a date, such as the age of a particular rock or process.

Figure 5b shows Y-content in monazite vs. calculated date for the same sample. Horizontal lines are 2σ uncertainties associated with the calculated date. These are shown here to give a sense of the magnitude of uncertainty but are omitted in subsequent figures; relative errors can be seen on the histogram plots in each figure. Figures 5c shows the same data as Fig. 5b but with arrows connecting the core and rim analyses of single monazite grains. These provide a constraint on relative age even when calculated uncertainties overlap. Figure 5d shows the sum of heavy rare earth elements (HREEs) in monazite vs. calculated date with arrows connecting cores and rims. HREEs and Y are strongly partitioned into garnet. Y has been used in many studies to link monazite growth with garnet growth and breakdown (see references in Williams et al., 2007). The characteristic 'U-shaped' profiles in Figure 5 b,c,d are interpreted to result from significant garnet growth at ca. 1150 Ma and garnet breakdown after ca. 1000 Ma. Downward plunging arrows at ca. 1150 Ma indicate significant garnet growth at this time. The HREE, and to some degree Y, show a small decrease between 1150 Ma and 1050 Ma This suggests some additional garnet growth after 1150 Ma, but from this plot, it is not possible to know when this garnet growth occurred within this 100 Ma window.

Figure 5e shows U content in monazite vs. calculated date. Like Y and HREEs, U decreases dramatically prior to 1150 Ma, from as high as 8000 ppm to 2000-3000 ppm. Unlike Y and HREEs, however, there is no late-stage increase in U; all subsequent monazite grains have the low U value with very little variation. Partitioning data from Stepanov et al. (2012) indicate that the actinides (U, Th) have positive monazite/melt fractionation, but U has a significantly lower ratio than Th and most REEs. During partial melting U and other trace and REEs will be partitioned from the whole rock into melt. Monazite in equilibrium with the melt will be depleted in uranium relative the other actinides or REEs, and if melt is extracted from the system, monazite in the residue will be expected to equilibrate with the lower bulk-rock uranium abundance. The decrease in U in monazite in sample 16TG-154 is thus, interpreted to result from partial melting of the sample. The fact that this reduction occurred at the same time as the Y and HREE reduction is consistent with melting by reactions 1 and 2 where garnet is produced as a peritectic phase during melting. The fact that the U content of monazite remains low during cooling and during subsequent events is taken as evidence that a large component of the melt was removed from the local system (see discussion below), consistent with the abundant K-feldspar and garnet and lack of plagioclase.

Figure 5f shows the Th-content in monazite for sample 16TG-154. Interestingly, Th content does not show a dramatic decrease during the proposed melting event at ca. 1150 Ma, nor does it show an increase after 1050Ma. Instead relative high-Th monazite grains tend to decrease in Th while relatively low-Th grains tend to increase. This “averaging” effect has been seen in several samples, and is taken to indicate the strong preference for Th in monazite relative to the solid rock or the melt phase and that later monazite are, at least in part, derived from earlier monazite. The dissolution of early high- or low-Th monazite tends to result in growth of new monazite with a more or less average Th composition. Even though the sample is interpreted to have lost a significant melt component, the Th content has remained nearly constant.

Sample 16TG-150 Elephant Rock. Figure 6a shows monazite dates from sample 16TG-150. Most monazite grains contain a high-Y core domain and a lower-Y outer “main” domain, although some grains consist entirely of the low-Y domain. High-Y rim domains are rare and narrow, and none were thick enough and homogeneous enough to be analyzed. Several matrix grains display a dramatically higher-U rim domain that is not present on monazite inclusions in garnet. Importantly, these domains tend to have irregular inner boundaries with the main monazite domain, and are interpreted to be monazite produced by a dissolution reprecipitation process (see Williams et al., 2011).

Figure 6b shows Y-concentration vs. date in sample 16TG-150 and Figure 6c shows HREEs in monazite. The monazite population is characterized by a dramatic decrease in Y and in HREE at ca. 1150 Ma. The lowest Y and HREE contents in 1150 Ma monazite are comparable to the contents in 1050 Ma monazite. Some grains show a decrease between 1150 cores and 1050 Ma rims, but from the trends in the overall population, we suggest that this change occurred primarily at 1150 Ma. That is, unlike sample 16TG-154 (and sample 16TG-151- below), only a minimal decrease in Y or HREE may have occurred after1150 Ma. We interpret this to indicate that most of the garnet in the sample grew by approximately 1150 Ma and thus, most of the melting (Reactions 1 and 2) occurred by this time.

In contrast to sample 16TG-154, the U content of monazite in 16TG-150 did not dramatically decrease at 1150 Ma (Fig. 6e). Instead, U shows the averaging effect described above, where for example, high-U cores have lower U rims and low-U cores have higher U rims. The trends suggest that younger monazite grew with a U-content similar to the average of that in the older grains. We take this to suggest that a significant amount of melt was not removed from this sample. Instead, melt formed and crystallized within the system. Monazite and U dissolved during melting, and upon crystallization, U was available to be incorporated into new monazite as it crystallized from melt. Th content behaves similarly to U except that the Th content appears to converge on values on the high-side of the average Th value. This may reflect the high compatibility of Th in monazite (Stepanov et al., 2012). As older monazite dissolves, Th is largely partitioned into younger monazite, i.e. compared to partial melt or any other minerals. The late-stage high-U monazite rims that occur only on matrix monazite grains are the exception to the above trends. They have much higher U content than any other grains in this or any of the samples studied here. The U is interpreted to have been introduced by hydrothermal fluids.

Sample 16TG-151 - Treadway Mountain. Monazite date-composition relationships in sample 16TG-151 (Fig. 7) show some distinct differences from the above samples. Both Y and HREEs decrease significantly at ca. 1150 Ma, consistent with a significant period of garnet growth at this time. Yttrium and HREEs increase after 1000 Ma, consistent with garnet breakdown; garnet is particularly anhedral in this sample (Fig. 2,3). However, there is considerably more variability in monazite composition at ca. 1050 Ma than in either of the above samples. Importantly, several monazite grains show a distinct decrease in Y and HREEs at ca, 1050 Ma., a behavior not observed in either of the above samples. This second reduction in Y and HREEs may indicate a second period of garnet growth, although we have not recognized textural or compositional evidence for distinct garnet generations.

Uranium in sample 16TG-151 shows fairly little change from 1150 through 1050 Ma. There is some evidence for the averaging effect (that is, grain-to-grain variability decreases in younger monazite) and possibly a slight decrease in U is apparent after 1000 Ma. This is distinctly different from the trend in 16TG-154 where U was depleted at ca. 1150 Ma. Thorium shows the decrease in variability in younger grains and also shows a distinct decrease in the youngest grains, i.e. younger than 1000 Ma. At least in these Adirondack Mountain samples, Th is retained in monazite during garnet growth and melting. However, Th has been known to decrease during fluid related or hydrothermal alteration/recrystallization (Williams et al., 2011), which may explain the decrease in the youngest rim domains.

Two grains (M-3 and M-19) illustrate the behavior in this sample particularly well (Figure 8, 9). Monazite grain #3 has eight distinct domains (Fig. 8a); it is possible to distinguish several core and several rim domains. HREEs drop at ca 1150 from the innermost core to the outer core domain. HREES are relatively constant to the outermost core domain (1060 Ma), followed by a second decrease in Y and HREEs at approximately 1060-1050 Ma (Fig. 8). This decrease is taken to be a second period of garnet growth at ca. 1050 Ma. The relatively constant Y and HREEs in grain 3 from 1150 to 1060 suggests that there was relatively little garnet growth (or breakdown?) during this 100 m.y. period. Grain 19 has no domains in the 1150 Ma range, but has at least nine domains that are ca. 1060 and younger (Figure 9). This grain documents the progressive decrease in Y and HREEs at ca. 1050. The fact that U also decreases at this time is taken to indicate further melting, probably by a reaction such as Reaction 1and/or 2. Th remains relatively constant through all phases of grain-19 growth (Fig. 8b- e), probably reflecting the strong partitioning of Th into monazite even in the presence of melt. The decrease in Th in the final two rim generations is consistent with these events involving fluid alteration (Williams et al., 2011). Eu decreases slightly during the growth of grain 19. This may reflect Eu partitioning into K-feldspar during melting by reactions 1 and 2.

Sample 16TG-153 – Swede Mountain Quartzite. A sample of aluminous quartzite, locally called “Dixon schist” (Ailling, 1916), was collected from within several meters of sample 16TG-154 (above). The sample is a schistose quartzite with the assemblage: Qtz, Grt, Sil, Pl, Ksp, Bt, graphite. Although some melting may have occurred, it is not interpreted to have undergone significant partial melting, and thus is not included in the primary data set that is used to constrain the conditions and timing of partial melting. However, several observations offer insight into the results summarized above.

No detrital or early metamorphic (Elzevirian?) monazite grains were recognized in the sample. However, the sample contains several monazite cores that are among the oldest (ca. 1200-1150 Ma) monazite in any of the samples studied here. Importantly, two cores (m11: 1184 +/- 30 Ma, m14: 1176 +/- 6 Ma) have very low Y-content. Both of these grains are surrounded by rims of nearly the same age that have much higher Y-content. Slightly younger monazite grains (ca. 1160-1150 Ma) have lower-Y content. Thus, although the dates overlap within error, core-rim relations suggest a low-high-low Y character to the ca. 1180-1150 Ma monazite.

We suspect that these old monazite cores grew during prograde Shawinigan metamorphism and their low-Y character may suggest that another Y-bearing phase (probably xenotime or allanite) was present in the early assemblage. The high-Y outer cores, are interpreted to reflect the breakdown of xenotime during prograde metamorphism. The subsequent decrease in Y is interpreted to reflect the growth of garnet, but unlike the other samples in this study, the garnet growth reaction is interpreted to have been a solid state one, involving the subsolidus breakdown of phyllosilicates.

Fabric Relationships

Monazite inclusions in garnet in sample 16TG-154 are distinct in texture from matrix grains (Fig. 10). Monazite grains included in garnet are sub-rounded and are weakly aligned perpendicular to the main migmatitic fabric (Fig. 10b). Matrix monazite grains are distinctly elongate and aligned parallel to the main fabric (Fig. 10b). Close inspection shows that the elongate part of the matrix monazite is the low-Y “outer core” domain, e.g. the rims on monazite grain 22 (Fig. 10). In this sample, the “main” (lowest-Y) domains are **not** distinctly preferentially developed around the grains. Similarly, the narrow high-Y rims are **not** preferentially developed on specific quadrants of the grains. This suggests that the main fabric in this sample may be more synchronous with the ca. 1150 Ma monazite than with the ca. 1050 Ma main generation or the rims. The location of the rim domains may be more controlled by fluid access along the grain boundary network rather than by any active deformation.

The distribution of garnet in the sample 16TG-154 may also provide insights into timing of mineral growth, especially feldspar, and also may be a useful kinematic indicator. Garnet crystals tend to occur in pairs or stacks dipping from upper left to lower right (Fig. 10 and inset). No stacks occur with the opposite sense. We suggest that the garnet became imbricated during top-right (top-west in true coordinates), thrust-sense shear in this sample. This sense of shear is consistent with local σ tails and weakly defined C’ structures in the sample. Importantly, the stacked garnet crystals are wrapped by, and engulfed in, relatively blocky, undefomed (i.e. non-recrystallized) K-feldspar, and as noted, K-feldspar locally forms σ tails on garnet. We take this to suggest that the K-feldspar crystallized during shearing and during imbrication of garnet, and thus, that the reaction that produced both K-feldspar and garnet occurred syntectonically.

Matrix monazite grains in sample 16TG-150 are also more elongate and oriented parallel to the main migmatitic fabric. In addition, the main low-Y domains are irregular in shape and tend to engulf matrix minerals as static rather than syntectonic overgrowths. As with sample 16TG-154, we interpret the main migmatitic fabric to have developed at the same time as the ca. 1150 Ma monazite generation. The younger (ca. 1050 and younger) monazite is interpreted to have grown statically.

Discussion

At least three regional tectonothermal events have been recognized in the Adirondack Highlands: the (1190-1140 Ma) Shawinigan orogeny, the (1090-1020 Ma) Ottawan orogeny, and to some degree, the (1010-980 Ma) Rigolet stage/orogeny (Rivers, 2008; McLelland et al., 2013; Chiarenzelli et al., 2017). One of the major challenges for interpreting the tectonic history of the region involves placing fabrics, textures, and metamorphic assemblages into the context of these events. This is particularly true for the Shawinigan and Ottawan orogenies, which have both been interpreted to involve granulite facies metamorphism, partial melting, and penetrative deformation (Heumann et al., 2006; Bickford et al., 2008; McLelland et al., 2013). Monazite domains from this study have yielded dates in each of the main age ranges including abundant data that span the (ca. 1160-1140 Ma) time of AMGC plutonism. Compositional mapping and composition-date relationships provide a number of insights into the significance of the monazite generations and into the tectonic history of the region in general.

In the following discussion, dates and interpreted ages will be shown mainly without uncertainties for brevity and clarity. Errors on most monazite dates are on the order of 4-15 m.y. and the two major granulite facies events are separated by approximately 100 m.y. (Shawinigan: 1190-1140 Ma vs. Ottawan: 1090-1020 Ma). All monazite dates and compositional analyses, with uncertainties, are provided in the supplemental documents. For the following discussion, the Shawinigan/AMCG event will be considered to be ca. 1150 Ma and the Ottawan event will be considered to be ca. 1050 Ma.

Early High-Y Monazite

The oldest monazite domains, present in all migmatite samples, are ca. 1180-1170 Ma. They tend to be either inclusions in garnet or irregularly-shaped cores surrounded by younger domains. They typically have the highest Y and HREE contents, suggesting that garnet was less abundant at the time that these monazite grains crystallized. There is little evidence preserved in these rocks concerning the reactions that produced these early high-Y monazite grains. However, in one quartzite sample (16TG-153) and several other samples from the eastern Adirondack Highlands, older monazite core domains (ca. 1180 Ma) have low Y contents, locally overgrown by high-Y outer cores. We suspect that these early grains may have equilibrated with xenotime (YPO_4), which would preferentially incorporate Y over monazite. If so, the origin of the early high-Y monazite in this study may involve the breakdown of xenotime or allanite during Shawinigan prograde metamorphism. Several core domains in 16TG-151 are even older (ca. 1225 Ma). We suspect that these may be remnants of the Elzevirian orogeny, but there are two few of these domains in this sample suite to draw firm conclusions.

Partial Melting at 1160-1150 Ma

Sample 16TG-154 (Swede Mountain) contains the silicate assemblage Sil-Grt-Ksp-Qtz-Bt (retrograde). It is interpreted to reflect the almost complete progression of reactions 1 and 2. That is, biotite and plagioclase were consumed, and the final assemblage is dominated by the solid products of incongruent melting reactions (garnet and K-feldspar). The lack of plagioclase-bearing (leucosome) domains, and the stability of the product assemblage (garnet and K-feldspar) suggests that partial melt was lost from the system, resulting in a residual bulk composition. Monazite is characterized by a dramatic decrease in Y, HREEs, and U at approximately 1160 to 1150 Ma. The average Y-content for all monazite grains older than 1160 Ma is approximately 7500 ppm (Fig. 5). The average Y-content for all grains in the 1160-1150 range is approximately 2000 ppm. Y and HREE content rebound after approximately 1050 Ma, but U content remains low and relatively constant. We suggest that U was partitioned into partial

DOI: https://doi.org/10.2138/am-2019-6906

melt and was lost from the system. Y and HREE were partitioned into garnet, and were released when garnet began to break down after 1050 Ma.

Results from sample 16TG-154 indicate that the dominant period of melting occurred at approximately 1160-1150 Ma and that a significant amount of garnet was produced at this time. Importantly, this period of time overlaps with the AMGC plutonism, near the end of the Shawinigan orogeny. In fact, from all of the samples investigated in this study, the peak of garnet production was in the range 1155-1150 Ma. Heating from AMGC intrusions and associated gabbroic intrusions may have contributed to the high temperature of metamorphism and may help to explain the abundance of migmatite in paragneiss across the Adirondack Highlands. The question of whether migmatite was related to the Shawinigan or Ottawan orogeny has been a major question to many workers. However, as also suggested by Heumann et al. (2006), these samples suggest that intrusion of the AMCG suite may have been an important time of melting.

Many workers have concluded that monazite is soluble in silicate melts, and thus, that monazite is expected to dissolve during partial melting (Kelsey et al. 2008; Rubatto et al. 2013; Harley and Nandakumar, 2014; Yakymchuk and Brown 2014; Yakymchuk, 2017). Certainly, the small size and anhedral shape of monazite grains older than 1150 Ma supports this idea. Further, old monazite domains are larger and more abundant when included in garnet as compared to matrix grains. However, the presence of ca. 1160-1150 Ma monazite with decreasing U, Y, and HREEs suggests that some monazite was able to crystallize during the partial melting process. There are several possible interpretations. First, some compositions of monazite may be in equilibrium with some partial melts. The positive partition coefficient for Th, U, and some other light REEs may suggest that some Th- and U-bearing monazite may be stable (see also Yakymchuk et al., 2018). This would be supported by the somewhat increasing Th content of younger monazite in the samples studied here. However, it also seems possible that the partial melting process is not a steady state homogeneous process (see Rubatto et al., 2013; Harley and Nandakumar, 2014; Wang et al., 2017). Local domains may melt while in others, melt may crystallize, depending on the local distribution of incompatible components and especially water. If so, monazite could be crystallizing in one part of a rock and dissolving in another as heterogeneous partial melting proceeds.

Samples collected from Elephant Rock, 1.5 km east, and from Treadway Mountain, 2 km west of the above sample also support a major period of partial melting at ca. 1160-1150 Ma. Both localities show a decrease in Y and HREE in monazite just prior to 1150 Ma, interpreted to reflect garnet production during melting by reactions 1 and 2. The fact that biotite occurs mainly in garnet shadows and the large magnitude of the Y and HREE decrease suggests that melting may have been more extensive in 16TG-150 and in fact, biotite may have been nearly consumed. The abundance of matrix biotite and lesser depletions of Y and HREE at Treadway Mountain (samples 16TG-151 a and b) suggest that melting may not have been as extensive there.

Importantly, monazite from both Elephant Rock and Treadway Mountain do not show the dramatic decrease in U that is seen at Swede Mountain. Instead, the U-content seems to show an averaging effect where low-U grains increase and high-U grains decrease, and the overall scatter decreases in subsequent grains. This suggests that, as older monazite grains dissolved and new monazite grains crystallized, the grains may have had a near equilibrium U content. Both samples converge on a value of approximately 5000 ppm U. The fact that these samples do not show a net loss of uranium, is taken to indicate that a significant component of U was not lost from the system during melting. Some U that was dissolved into the melt component was available for new monazite during melt crystallization. We suggest that the U behavior indicates that a smaller amount of melt, if any, was removed from these samples compared to 16TG-154.

Samples investigated from Treadway Mountain have a very different overall texture from the other two localities. These samples contain dispersed plagioclase, K-feldspar, and foliated biotite (Fig. 2,3). There are few, if any, leucosome tails adjacent to garnet, especially as compared to other localities. We suggest that melting occurred with little melt segregation, even into small-scale leucosome domains. On crystallization, garnet and K-feldspar were resorbed and biotite and plagioclase crystallized locally, perhaps even on existing crystals of the same mineral (Holness and Sawyer, 2008).

In summary, the three localities studied here show three different behaviors during melting. Sample 16TG-154 (Swede Mountain) experienced significant melting and a large percentage of the melt was removed from the local system. In sample 16TG-150 (Elephant Rock), partial melt was segregated locally but crystallized largely near the associated residue. In sample 16TG-151, little segregation occurred and melt domains crystallized largely in place. The three different styles were fundamentally important for the subsequent (Ottawan) metamorphic event (see below).

The Ottawan Orogeny

The Ottawan orogeny is interpreted to have occurred in the range 1090-1020 Ma, based on regional constraints (Rivers, 2008). However, some workers subdivide the event into an early prograde or peak phase (1090- ca.1060 Ma) and a later extensional phase (1060-1020 Ma) (Wong et al., 2012; Chiarenzelli et al., 2017). Peak conditions are estimated to have been in the granulite facies, perhaps similar to those in the Shawinigan orogeny (Spear and Markussen, 1997; Peck et al., 2018). Samples from Swede Mountain (16Tg-154) and Elephant Rock (16Tg-

150) have yielded essentially no monazite grains/domains with dates in the 1090-1060 range, and there is little evidence for new melting in these samples.

Sample 16TG-151 (Treadway Mountain) is very different. Numerous monazite domains and whole grains yielded dates in the 1090-1050 Ma range, especially between 1060 and 1050, the presumed prograde and peak phase of the Ottawan event. Importantly, numerous grains including M3 and M19 (Fig. 8a,b) show a core-to-rim drop in Y, HREEs, and U at this time, and there is some evidence for the averaging phenomenon of both U and Th content that is characteristic of melting. We interpret this to indicate new garnet growth and partial melting by reactions 1 and/or 2 at this time. So far, garnet compositional mapping and quantitative traverses have not definitively shown two distinct garnet compositions or textures. This may not be surprising because the Ottawan event is interpreted to have involved high temperatures (>800° C) (Spear and Markussen, 1997) and thus, rapid diffusion. Also, the operation of similar reactions at similar grades may have produced similar garnet compositions. Based on zircon analysis in leucosomes, Bickford et al. (2008) also suggested that the Treadway Mountain locality underwent some amount of melting during the Ottawan orogeny.

A full explanation for the differing behavior of the three samples during the Ottawan Orogeny must await additional analysis and more samples. Petrologic forward modeling using isochemical phase diagrams is underway to quantitatively model the melting process. However, current bulk compositions are similar, and all three rocks have lost at least some amount of partial melt, so these are residual bulk compositions that do not reflect the composition of the protolith. Original bulk compositional differences probably played a role in controlling the exact melting reaction and the degree of melting, especially at ca. 1160-1150 Ma. However, the dynamics of melt segregation and removal may have also played a role. Much of the ca. 1150

Ma melt from sample 16TG-154 was apparently removed and 16TG-150 underwent coarse compositional segregation. This apparently left both samples relatively infertile during the younger thermotectonic event. Sample 16-TG-151 may have undergone less melting during the earlier event, but it seems likely that any melt component remained dispersed in the rock producing a finer-grained and more homogeneous texture. After crystallization, the melt and residue components were more finely and evenly distributed in this sample, leaving it more fertile for the second melting event.

Retrograde Metamorphism

Monazite grains examined in this study, as well as monazite from around the eastern Adirondack Mountains, show evidence for retrograde metamorphism starting at approximately 1050 Ma. Yttrium and HREEs in monazite increase significantly in monazite domains younger than 1030 Ma. The increases are interpreted to reflect breakdown of garnet and release of HREES and Y. The Y- and HREE enriched domains typically occur as narrow rims, and are never present on grains completely enclosed in garnet. Unlike those shown by Wong et al., (2012), the rims observed here are not preferentially oriented and thus, may not be particularly syntectonic. Rocks described by Wong et al (2012) were interpreted to come from the East Adirondack shear zone, and to be related to orogenic collapse following the Ottawan orogeny. Rim domains from this study may reflect the same collapse event, but they were not specifically located within collapse-related structures.

All rocks examined in this study contain monazite grains with the high-Y/HREE rims. In fact, essentially all of the many 10's of samples examined from around the eastern Adirondack Highlands have at least some high-Y/REE monazite rims. Of the samples investigated in this study, the rims are most consistently developed in the Treadway Mountain samples, and are only

This is a preprint, the final version is subject to change, of the American Mineralogist (MSA)
Cite as Authors (Year) Title. American Mineralogist, in press.
DOI: https://doi.org/10.2138/am-2019-6906

present on several specific grains in the other localities. These samples have coarse, feldspar dominated leucosome domains that may have isolated monazite grains from late-stage fluids.

It is interesting that, although there is widespread preservation of early, ca. 1150 Ma and older, monazite cores, there are no high-Y/REE rim domains of this late-Shawinigan age. Orogenic collapse and exhumation have been interpreted to have occurred soon after the Shawinigan orogeny (Rivers, 2008; McLelland, 2013), and decompression/exhumation would be required if the 1155 Ma Marcy anorthosite was emplaced into shallow crust (Valley and O'Neill, 1982). However, there is essentially no monazite evidence for garnet break-down after 1150 Ma. Initially, one might suspect that for some reason, monazite did not record the post-Shawinigan decompression. Yet, monazite in these samples is very sensitive to decompression and garnet break-down after 1050 Ma. It is difficult to imagine that a major post-Shawinigan decompression event was not captured in any of the samples, but the post-Ottawan decompression event was captured in virtually every sample. This suggests that there may have been less post-Shawinigan (post 1150 Ma) decompression in the Adirondack Highlands than previously thought.

Several samples are characterized by decreasing Th in monazite domains younger than approximately 1000 Ma. This is particularly apparent in the Treadway sample 16TG-151. This seems contradictory to the interpretation that Th is strongly partitioned into monazite relative to melt or other major minerals (Stepanov et al., 2012; and see above). However, there is evidence that Th may be removed from monazite during fluid alteration by a dissolution reprecipitation mechanism (Putnis and Austrheim, 2010; Harlov and Hetherington, 2010 ; Williams et al., 2011). Several of the low-Th domains show textural evidence of alteration rather than overgrowth, for example, irregular low-Th domain boundaries cutting earlier domain boundaries (Fig. 8b) (see Williams et al., 2011). Dissolution reprecipitation may be particularly effective in the presence of alkaline fluids Harlov and Hetherington, 2010; Harlov et al., 2011). This would be consistent with the characteristic Na-metasomatism associated with late iron mineralization in the eastern Adirondacks (Valley et al., 2010; 2011). Thus, the late depleted Th signature may be a signal of the late hydrothermal phase in the evolution of the Adirondack Highlands.

Timing of Deformation

Textural evidence suggests that the main gneiss-forming deformational event in the samples studied was synchronous with partial melting at ca. 1160-1150 Ma. The K-feldspar-rich leucosome in the Swede Mountain restite sample represents the solid product of the peritectic melting reaction, and the Qtz-Pl-Ksp leucosome in the Elephant-Rock sample show evidence for pooling of leucosome (melt?) in garnet shadows. Also, imbricated garnet in the Swede Mountain sample that is wrapped by annealed K-feldspar suggest flow of garnet crystals during melt-present flow. The ca. 1150 Ma monazite domains are distinctly aligned in the main migmatite layering, especially at Swede Mountain. These domains probably reflect local melt crystallization, and they support the interpretation of syn-melting deformation. Older monazite inclusions in garnet are not aligned in the migmatitic fabric and in fact, may have a slight preferred orientation perpendicular to this main fabric. Late-stage monazite domains (>1050 Ma) also lack a preferred orientation. This is in contrast to the late domains farther east where late collapse-related strain has been interpreted (Wong et al., 2012). We suggest that the high temperatures and presence of partial melt contributed to melt-weakening and deformation at ca. 1150 Ma and further, although the sample records the late-stage (ca. 1050-1000 Ma) decompression, the locality was not actively deforming at this time.

Sample 16TG-151 (Treadway Mountain) has a gneissic fabric in hand specimen, but individual minerals are only weakly foliated. Biotite books are moderately well aligned, but plagioclase and K-feldspar grains have only a weak preferred orientation. Most feldspar crystals have an irregular sub-equant shape. This texture probably developed during crystallization of the small amount of melt that had formed during the second (i.e. 1050 Ma) melting event. The weak foliation does suggest some reactivation at ca. 1050 Ma in these melt-weakened rocks.

Mineral lineations and kinematic indicators are poorly developed in all of the migmatite samples. This is in distinct contrast to the one meta-quartzite sample (16TG-153), which has a strong mineral lineation. We suspect that the melt-weakened rocks at ca. 1150 Ma were not particularly amenable to lineation formation, but it is possible that some annealing occurred during later (Ottawan) orogenesis. Pooling of leucosome, possible imbrication of garnet, and subtle shear bands provide a low-confidence top-west sense of shear. This is opposite of the sense interpreted for the (ca. 1050-1030 Ma) East Adirondack shear system along the eastern edge of the uplift (Wong et al., 2012) and may characterize Shawinigan deformation (thrusting?) in this area.

Implications

Partial melting can play a key role in the tectonic history of orogenic belts (eg. Hollister and Crawford, 1986; Hollister, 1993). Melting events can lead to weakening and thus, deformation of the crust and strengthening again when the melts crystallize. In addition, melting events record thermal perturbations that can have large-scale geodynamic significance. It is critical to constrain the timing of melting and the relationship to deformation events and other tectonic events both before and after anataxis. Monazite is a powerful petrochronological tool for constraining the timing of metamorphism, melting, melt crystallization, and deformation.

The three samples/localities summarized here are similar in appearance. They are all garnet-rich migmatitic grey gneisses. But compositional maps and the monazite record suggest that they have very different petrologic, microstructural, and tectonic histories, especially with regard to melting and melt loss. Sample 16TG-154 (Swede Mountain) experienced significant melting at ca. 1150 Ma and melt loss with little garnet growth or melting occurred during the Ottawan orogeny (ca. 1090-1050 Ma). Monazite in sample 16TG-150 (Elephant Rock) suggests that melting also occurred at ca. 1150 Ma, but rather than being lost from the local system, the melt and restite were segregated into coarse plagioclase-rich (former melt) and K-feldspar-rich (solid products) layers. Sample 16TG-151 shows evidence for garnet growth and melting at 1150 Ma and also at 1050 Ma. Although some melting apparently occurred at 1150 Ma, the melt component is interpreted to have remained largely in place and not segregated into leucosome layers. Consequently, this sample was more fertile for melting during the Ottawan Orogeny. A major implication is that, in polymetamorphic regions such as this, the physical and chemical character of earlier events can have a significant impact on the degree of melting (and melt-weakening) during later events.

All three samples investigated in this study have a strong, shallowly-dipping foliation and weakly developed to nonexistent lineation. It would be tempting to correlate this fabric from locality to locality, especially in these three closely-spaced localities. However, based on the fabric and monazite record, samples 16TG-150 and 16TG-154 largely preserve their 1150 Ma migmatitic fabric while the fabric in 16TG-151 was reactivated at 1050 Ma. The Shawinigan Orogeny apparently involved crustal thickening culminating in partial melting at ca. 1160-1150 Ma (Rivers, 2008; McLelland et al., 2013). The associated melt weakening is interpreted to have led to the subhorizontal migmatitic fabric preserved in samples 150 and 154. Both samples do have subtle evidence for west-directed shearing. We suggest that at ca. 1050 Ma localized melting in certain fertile localities led to a second phase of melt weakening and fabric development roughly parallel to the preexisting fabric. Although kinematic indicators are not strongly developed, sample 16TG-151 has the least evidence for non-coaxial strain. This may be the result of reactivation during the Ottawan orogeny.

All three of the samples described here show little evidence for oriented monazite growth during the development of late rims (ca. 1060-980 Ma). This is a distinct contrast to samples further east in the Adirondack highlands (Wong et al., 2012) or samples near the margin of the Marcy Anorthosite (Regan et al., 2019), both of which have been interpreted to have been active during the extensional collapse of the Ottawan orogeny. Apparently the samples described here record the late decompression and garnet break-down and also fluid alteration, but they are not located within, or associated with, a structure that accommodated the collapse.

One would hope to be able to map, in the field, the effects of Shawinigan vs. Ottawan metamorphism and the effects of Shawinigan vs. Ottawan deformation. However, as noted, the three samples investigated here are extremely similar in terms of outcrop appearance, fabrics and kinematics. All three samples experienced Shawinigan garnet growth, melting, and deformation, but only sample 16TG151 (Treadway Mountain) experienced significant Ottawan melting and deformation. At least for these grey gneisses, compositional mapping, detailed monazite analysis, and the integration of results from multiple samples is necessary to extract the full history.

Acknowledgements

Funding for this project came from NSF Grant EAR-1419876 to Williams and Grover. The authors would like to thank Jeff Chiarenzelli, Chris Yakymchuck, and an anonymous reviewer for careful and very helpful reviews. We thank Associate Editor, Callum Hetherington

DOI: https://doi.org/10.2138/am-2019-6906

for helpful comments and for his handling of the manuscript. We also thank Greg Dumond for his careful review of an earlier version of the paper. In addition, we sincerely thank Greg Walsh, Graham Baird, Jim McLelland, Pat Bickford, Peter Valley, and Felix Gervais for many discussions and insights into Adirondack and Grenville geology. We would particularly like to thank Bruce Selleck for discussion, encouragement, and friendship. Bruce will be dearly missed in the Adirondacks.

References Cited

Allaz, J.M., Williams, M.L., Jercinovic, M.J., Goemann, K., and Donovan, J. (2019) Multipoint Background Analysis: Gaining Precision and Accuracy in Microprobe Trace Element Analysis. Microscopy and Microanalysis, 25(1), 30-46.

Alling, H.L. (1916) Glacial Lakes and other glacial features of the central Adirondacks. Geological Society of America Bulletin, 27, 645-672.

Bickford, M.E., McLelland, J.M., Selleck, B.W., Hill, B.M., and Heumann, M.J. (2008) Timing of anatexis in the eastern Adirondack Highlands: Implications for tectonic evolution during ca. 1050 Ma Ottawan orogenesis. Geological Society of America Bulletin, 120(7-8), 950-961.

Bohlen, S.R., Valley, J., and Essene, E.J. (1985) Metamorphism in the Adirondacks. I. Petrology, Pressure and Temperature. Journal of Petrology, 26(4), 971-992.

Buddington, A.F. (1939) Adirondack igneous rocks and their metamorphism. Geological Society of America Memoir - 7, 354.

Cherniak, D.J., Watson, E.B., Grove, M., and Harrison, T.M. (2004) Pb diffusion in monazite: a combined RBS/SIMS study. Geochimica et Cosmochimica Acta, 68, 829-840.

Chiarenzelli, J., Lupulescu, M., Thern, E., and Cousens, B. (2011) Tectonic implications of the discovery of a Shawinigan ophiolite (Pyrites Complex) in the Adirondack Lowlands. Geosphere, 7(2), 333-356.

Chiarenzelli, J., Regan, S., Peck, W.H., Selleck, B.W., Cousens, B., Baird, G.B., and Shrady, C.H. (2010) Shawinigan arc magmatism in the Adirondack Lowlands as a consequence of closure of the Trans-Adirondack backarc basin. Geosphere, 6(6), 900-916.

Chiarenzelli, J., Selleck, B., Lupulescu, M., Regan, S., Bickford, M.E., Valley, P., and McLelland, J.M. (2017) Lyon Mountain ferroan leucogranite suite: Magmatic response to extensional thinning of overthickened crust in the core of the Grenville orogen. Geological Society of America Bulletin, 129(11-12), 1472-1488.

Chiarenzelli, J., Valentino, D., Lupulescu, M., Thern, E., and Johnston, S. (2011) Differentiating Shawinigan and Ottawan orogenesis in the Central Adirondacks. Geosphere, 7(1), 2-22.

Dumond, G., Goncalves, P., Williams, M.L., and Jercinovic, M.J. (2015) Monazite as a monitor of melting, garnet growth and feldspar recrystallization in continental lower crust. Journal of Metamorphic Geology, 33(7), 735-762.

Hamilton, M.A., McLelland, J.M., and Selleck, B. (2004) SHRIMP U-Pb zircon geochronology of the anorthosite-mangerite-charnockite-granite (AMCG) suite, Adirondack Mountains, New York: Ages of emplacement and metamorphism. In R.P. Tollo, L. Corriveau, J. McLelland, and M.J. Bartholomew, Eds. Proterozoic tectonic evolution of the Grenville orogen in North America, p. 337-355. Geological Society of America Memoir 197.

Hanmer, S., and Passchier, C.W. (1991) Shear-sense indicators: A review. Geological Survey of Canada Paper, 90-17.

Harley, S.L., and Nandakumar, V. (2014) Accessory Mineral Behaviour in Granulite Migmatites: a Case Study from the Kerala Khondalite Belt, India. Journal of Petrology, 55(10), 1965-2002.

Harlov, D.E., and Hetherington, C.J. (2010) Partial high-grade alteration of monazite using alkali-bearing fluids: Experiment and nature. American Mineralogist, 95(7), 1105-1108.

Harlov, D.E., Wirth, R., and Hetherington, C.J. (2011) Fluid-mediated partial alteration in monazite: the role of coupled dissolution–reprecipitation in element redistribution and mass transfer. Contributions to Mineralogy and Petrology, 162(2), 329-348.

Heumann, M.J., Bickford, M.E., Hill, B.M., McLelland, J.M., Selleck, B.W., and Jercinovic, M.J. (2006) Timing of anatexis in metapelites from the Adirondack lowlands and southern highlands: A manifestation of the Shawinigan orogeny and subsequent anorthosite-mangerite-charnockite-granite magmatism. Geological Society of America Bulletin, 118(11-12), 1283-1298.

Hollister, L.S. (1993) The Role of melt in the uplift and exhumation of orogenic belts. Chemical Geology, 108(108), 31-48.

Hollister, L.S., and Crawford, M.L. (1986) Melt-enhanced deformation: A major tectonic process. Geology, 14, 558-561.

Holness, M.B., and Sawyer, E.W. (2008) On the Pseudomorphing of Melt-filled Pores During the Crystallization of Migmatites. Journal of Petrology, 49(7), 1343-1363.

Jercinovic, M.J., Williams, M.L., and Lane, E., D. (2008) In-situ trace element analysis of monazite and other fine-grained accessory minerals by EPMA. Chemical Geology, 254, 197-215.

Kelsey, D.E., Clark, C., and Hand, M. (2008) Thermobarometric modelling of zircon and monazite growth in melt-bearing systems; examples using model metapelitic and metapsammitic granulites. Journal of Metamorphic Geology, 26(2), 199-212.

Kelsey, D.E., and Hand, M. (2015) On ultrahigh temperature crustal metamorphism: Phase equilibria, trace element thermometry, bulk composition, heat sources, timescales and tectonic settings. Geoscience Frontiers, 6(3), 311-356.

DOI: https://doi.org/10.2138/am-2019-6906

Koblinger, B.M., and Pattison, D.R.M. (2017) Crystallization of Heterogeneous Pelitic Migmatites: Insights from Thermodynamic Modelling. Journal of Petrology, 58(2), 297-326.

Korhonen, F.J., Clark, C., Brown, M., and Taylor, R.J.M. (2014) Taking the temperature of Earth's hottest crust. Earth and Planetary Science Letters, 408(0), 341-354.

Lupulescu, M.V., Chiarenzelli, J.R., Pullen, A.T., and Price, J.D. (2011) Using pegmatite geochronology to constrain temporal events in the Adirondack Mountains. Geosphere, 7(1), 23-39.

McLelland, J., Daly, J.S., and McLelland, J.M. (1996) The Grenville orogenic cycle (ca. 1350-1000 Ma); an Adirondack perspective. Tectonophysics, 265(1-2), 1-28.

McLelland, J., Hamilton, M., Selleck, B., McLelland, J., Walker, D., and Orrell, S. (2001) Zircon U-Pb geochronology of the Ottawan Orogeny, Adirondack Highlands, New York: regional and tectonic implications. Precambrian Research, 109(1), 39-72.

McLelland, J.M., Bickford, M.E., Hill, B.M., Clechenko, C.C., Valley, J.W., and Hamilton, M.A. (2004) Direct dating of Adirondack massif anorthosite by U-Pb SHRIMP analysis of igneous zircon: Implications for AMCG complexes. Geological Society of America Bulletin, 116(11-12), 1299-1317.

McLelland, J.M., Bickford, M.E., Spear, F.S., and Storm, L.C. (2002) Geology and Geochronology of the Eastern Adirondacks. New York State Geological Association Field Trip Guide Trip B1.

McLelland, J.M., Selleck, B.W., and Bickford, M.E. (2013) Tectonic Evolution of the Adirondack Mountains and Grenville Orogen Inliers within the USA. Geoscience Canada, Harold Williams Series, 40(4).

McLelland, J.M., Selleck, B.W., Hamilton, M.A., and Bickford, M.E. (2010) Late- to post-tectonic setting of some major Proterozoic anorthosite – mangerite – charnockite – granite (AMCG) suites. The Canadian Mineralogist, 48(4), 729-750.

Mezger, K. (1992) Temporal evolution of regional granulite terranes: Implications for the formation of lowermost continental crust. In D.M. Fountain, R. Arculus, and R.W. Kay, Eds. Continental Lower Crust, p. 447-478. Elsevier, Amsterdam.

Montel, J., Foret, S., Veschambre, M., Nicollet, C., and Provost, A. (1996) Electron microprobe dating of monazite. Chemical Geology, 131, 37-53.

Peck, W.H., Selleck, B.W., Regan, S.P., Howard, G.E., and Kozel, O.O. (2018) In-situ dating of metamorphism in Adirondack anorthosite. American Mineralogist, 103(10), 1523-1529.

Putnis, A., and Austrheim, H. (2010) Fluid-induced processes: metasomatism and metamorphism. Geofluids, 10(1-2), 254-269.

Regan, S., Walsh, G.J., Williams, M.L., Chiarenzelli, J.R., Toft, M., and McAleer, R.J. (2019) Syn-collisional exhumation of hot middle crust in the Adirondack Mountains: implications for extensional orogenesis in the southern Grenville Province. Geosphere, 15.

Regan, S.P., Chiarenzelli, J.R., McLelland, J.M., and Cousens, B.L. (2011) Evidence for an enriched asthenospheric source for coronitic metagabbros in the Adirondack Highlands. Geosphere, 7(3), 694-709.

Rivers, T. (2008) Assembly and preservation of lower, mid, and upper orogenic crust in the Grenville Province—Implications for the evolution of large hot long-duration orogens. Precambrian Research, 167(3), 237-259.

Rubatto, D., Chakraborty, S., and Dasgupta, S. (2013) Timescales of crustal melting in the Higher Himalayan Crystallines (Sikkim, Eastern Himalaya) inferred from trace element-constrained monazite and zircon chronology. Contributions to Mineralogy and Petrology, 165(2), 349-372.

Selleck, B., McLelland, J.M., and Bickford, M.E. (2005) Granite emplacement during tectonic exhumation: The Adirondack example. Geology, 33(10), 781-784.

Spear, F.S., and Markussen, J.C. (1997) Mineral Zoning, P–T–X–M Phase Relations, and Metamorphic Evolution of some Adirondack Granulites, New York. Journal of Petrology, 38(6), 757-783.

Storm, L.C., and Spear, F.S. (2005) Pressure, temperature and cooling rates of granulite facies migmatitic pelites from the southern Adirondack Highlands, New York. Journal of Metamorphic Geology, 23(2), 107-130.

Valley, J.W., and O'Neil, J.R. (1982) Oxygen isotope evidence for shallow emplacement of Adirondack anorthosite. Nature, 300, 497.

Valley, P.M., Fisher, C.M., Hanchar, J.M., Lam, R., and Tubrett, M. (2010) Hafnium isotopes in zircon: A tracer of fluid-rock interaction during magnetite–apatite ("Kiruna-type") mineralization. Chemical Geology, 275(3), 208-220.

Valley, P.M., Hanchar, J.M., and Whitehouse, M.J. (2011) New insights on the evolution of the Lyon Mountain Granite and associated Kiruna-type magnetite-apatite deposits, Adirondack Mountains, New York State. Geosphere, 7(2), 357-389.

Wang, J.-M., Wu, F.-Y., Rubatto, D., Liu, S.-R., Zhang, J.-J., Liu, X.-C., Yang, L.J.C.t.M., and Petrology. (2017) Monazite behaviour during isothermal decompression in pelitic granulites: a case study from Dinggye, Tibetan Himalaya. 172(10), 81.

DOI: https://doi.org/10.2138/am-2019-6906

White, R.W., and Powell, R. (2002) Melt loss and the preservation of granulite facies mineral assemblages. Journal of Metamorphic Geology, 20(7), 621-632.

White, R.W., Powell, R., and Holland, T.J.B. (2007) Progress relating to calculation of partial melting equilibria for metapelites. Journal of Metamorphic Geology, 25(5), 511-527.

Williams, M.L., Jercinovic, M.J., Goncalves, P., and Mahan, K.H. (2006) Format and philosophy for collecting, compiling, and reporting microprobe monazite ages. Chemical Geology, 225, 1-15.

Williams, M.L., Jercinovic, M.J., Harlov, D.E., Budzyn, B., and Hetherington, C.J. (2011) Resetting monazite ages during fluid-related alteration. Chemical Geology, 283(3-4), 218-225.

Williams, M.L., Jercinovic, M.J., and Hetherington, C.J. (2007) Microprobe Monazite Geochronology: understanding geologic processes by integrating composition and chronology. Annual Reviews of Earth and Planetary Sciences, 35, 137-175.

Williams, M.L., Jercinovic, M.J., Mahan, K.E., and Dumond, G. (2017) Electron microprobe petrochronology. In M.J. Kohn, M. Engi, and P. Lanari, Eds. Petrochronology: Methods and Applications, 83, p. 153-182. Reviews in Mineralogy and Geochemistry v. 83

Wong, M.S., Williams, M.L., McLelland, J.M., Jercinovik, M.J., and Kowalkoski, J. (2012) Late Ottawan extension in the eastern Adirondack Highlands: Evidence from structural studies and zircon and monazite geochronology. Geological Society of America Bulletin, 124(5-6), 857-869.

Yakymchuk, C. (2017) Behaviour of apatite during partial melting of metapelites and consequences for prograde suprasolidus monazite growth. Lithos, 274–275, 412-426.

Yakymchuk, C., and Brown, M. (2014) Behaviour of zircon and monazite during crustal melting. Journal of the Geological Society, 171(4), 465-479.

Figure Captions

Figure 1. Generalized geologic map of the Adirondack Mountains (after McLelland et al., 2010). Gray color shows location of metasediments. Inset left show the location of the Adirondack Mountains in relation to the Canadian Grenville Province. Inset right show the location of the three outcrops from which samples were taken for this study.

Figure 2. Photomicrographs from the three main outcrops treated here: a,b – 16TG-154 Swede Mountain area, c,d – (16TG-150 Elephant Rock, e,f – 16TG-151 Treadway Mountain. Images in plane polarized (left) and cross polarized (right) light. See text for discussion.

Figure 3. Full-thin-section compositional maps. Brighter colors indicate higher abundance of the particular element. For each element, the maps for the three samples have been processed simultaneously such that color intensities are comparable from map to map. Maps were collected with pixel size = 35µm, current = 300nA, dwell time = 25ms. See text for discussion.

Figure 4. Isochemical phase diagram pseudosection, for subaluminous pelite composition (from White et al., 2007 – Fig. 6). Yellow line shows the wet solidus. Red line shows the interpreted peak P-T conditions (and peak assemblages) for samples from this study.

Figure 5. Monazite composition relationships for sample 16TG-154 (Swede Mountain). (a) Gaussian distribution showing all monazite dates. Each distribution curve represents one monazite domain. (b, c): Yttrium vs date. Red arrows connect domains from single monazite grains; arrows point to outer (younger) domain. (d) sum of the heavy Rare Earth Elements vs.

date. Because of the sensitivity of the electron microprobe, these data are dominated by Gd and Dy. (e) Uranium vs. date. (f) Thorium vs date. Horizontal scales are equal in all figures. See text for discussion.

Figure 6. Monazite composition relationships for sample 16TG-154 (Swede Mountain). (a) Gaussian distribution showing all monazite dates. Each distribution curve represents one monazite domain. (b, c): Yttrium vs date. Red arrows connect domains from single monazite grains; arrows point to outer (younger) domain. (d) sum of the heavy Rare Earth Elements vs. date. Because of the sensitivity of the electron microprobe, these data are dominated by Gd and Dy. (e) Uranium vs. date. (f) Thorium vs date. Horizontal scales are equal in all figures. See text for discussion.

Figure 7. Monazite composition relationships for sample 16TG-151, Treadway Mountain. (a) Gaussian distribution showing all monazite dates. Each distribution curve represents one monazite domain. (b) Yttrium vs date. Red arrows connect domains from single monazite grains; arrows point to outer (younger) domain. (c) sum of the heavy Rare Earth Elements vs. date. (d) four particularly important monazite grains from figure 7c. Because of the sensitivity of the electron microprobe, these data are dominated by Gd and Dy. (e) Uranium vs. date. (f) Thorium vs date. Horizontal scales are equal in all figures. See text for discussion.

Figure 8. Monazite composition relationships for one monazite grain (m3) from sample 16TG-151, Treadway Mountain. (a) Y-Kα map and interpretive sketch of the monazite grain. (b) Gaussian distribution(s) showing all monazite dates from grain m3 with Yttrium vs date plot.

DOI: https://doi.org/10.2138/am-2019-6906

Red arrows connect domains from single monazite grains; arrows point to outer (younger) domain. (c) sum of the heavy Rare Earth Elements vs. date. (d) Uranium vs. date. Horizontal scales are equal in all figures. See text for discussion.

Figure 9. Monazite composition relationships for one monazite grain (m19) from sample 16TG-151, Treadway Mountain. (a) Y-Kα map and interpretive sketch of the monazite grain. (b) Gaussian distribution(s) showing all monazite dates from grain m19 with Yttrium vs date plot. Red arrows show trends from inner core to outer rim. (c) sum of the heavy Rare Earth Elements vs. date. (d) Uranium vs. date. (e) Thorium vs. date. (d) Europium vs. date. Horizontal scales are equal in all figures. See text for discussion.

Figure 10. Compositional maps for sample 16TG-154, Swede Mountain, with high-resolution monazite YKα grain maps superimposed. Dark lines connect grain maps to location of the monazite grain with the full section. (a) shows monazite grains included in garnet. (b) matrix monazite grains. See text for discussion.

This is a preprint, the final version is subject to change, of the American Mineralogist (MSA)
Cite as Authors (Year) Title. American Mineralogist, in press.
DOI: https://doi.org/10.2138/am-2019-6906

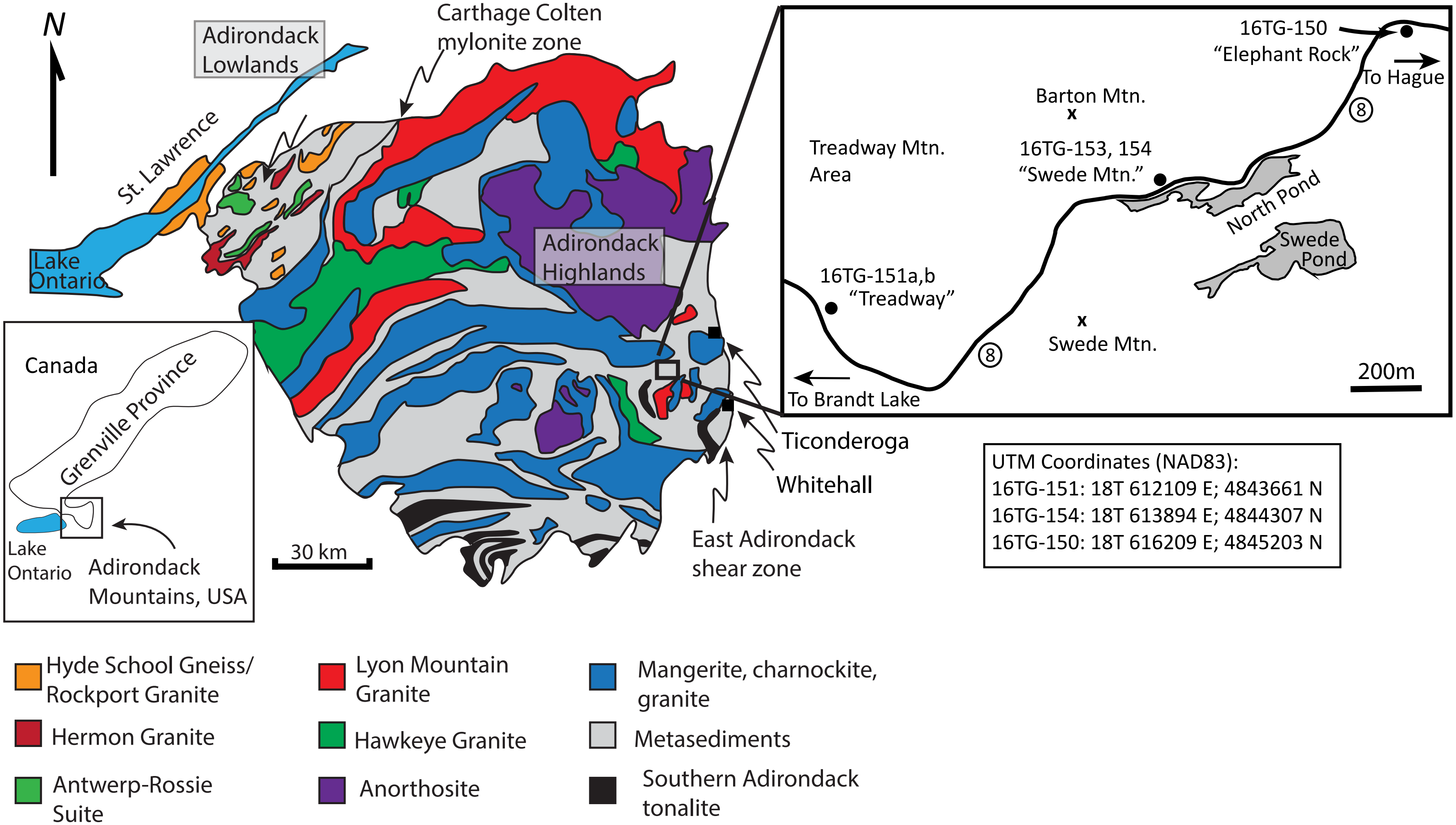

Fig. 1

This is a preprint, the final version is subject to change, of the American Mineralogist (MSA)
Cite as Authors (Year) Title. American Mineralogist, in press.
DOI: https://doi.org/10.2138/am-2019-6906

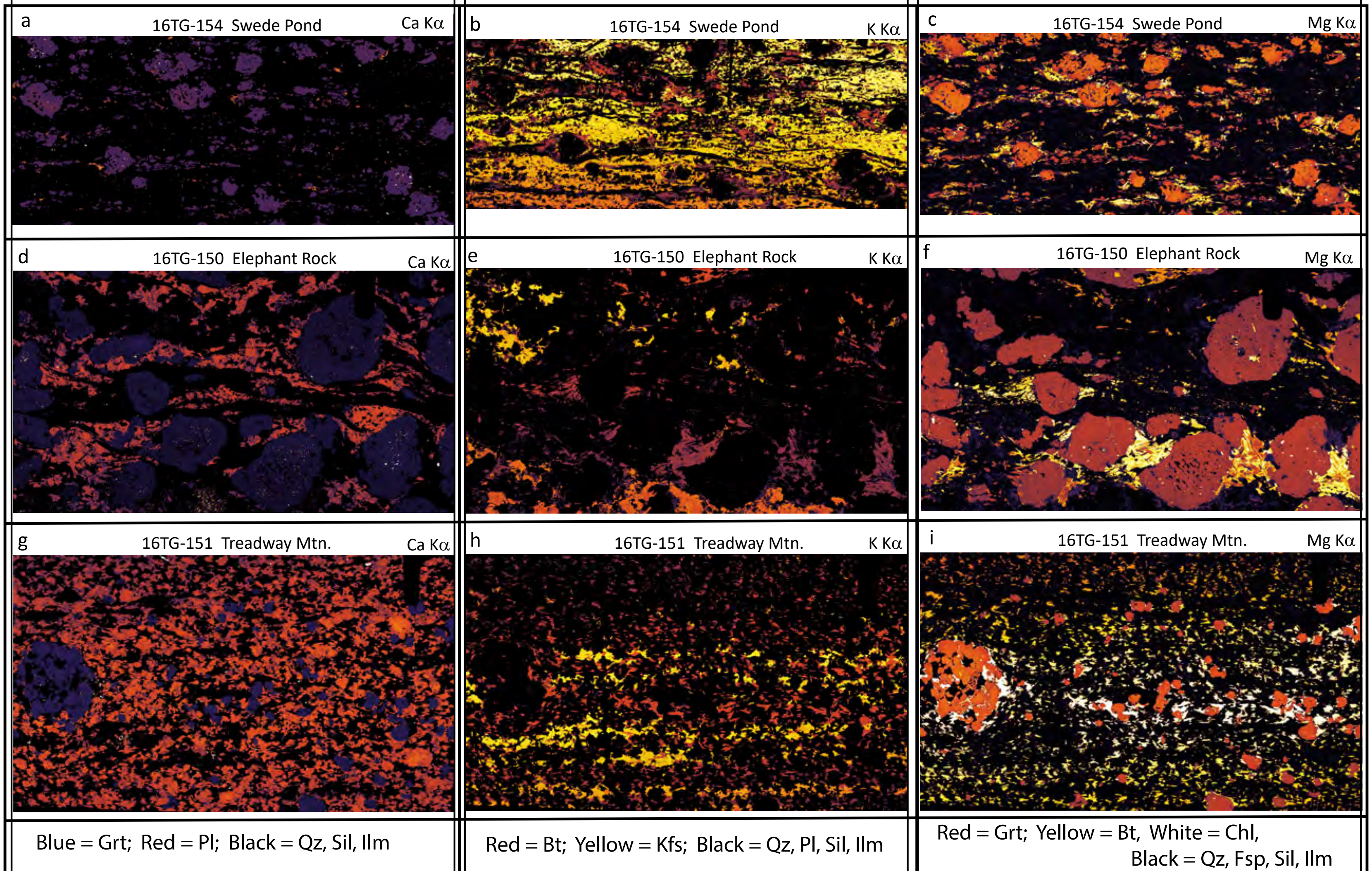

Fig. 3

DOI: https://doi.org/10.2138/am-2019-6906

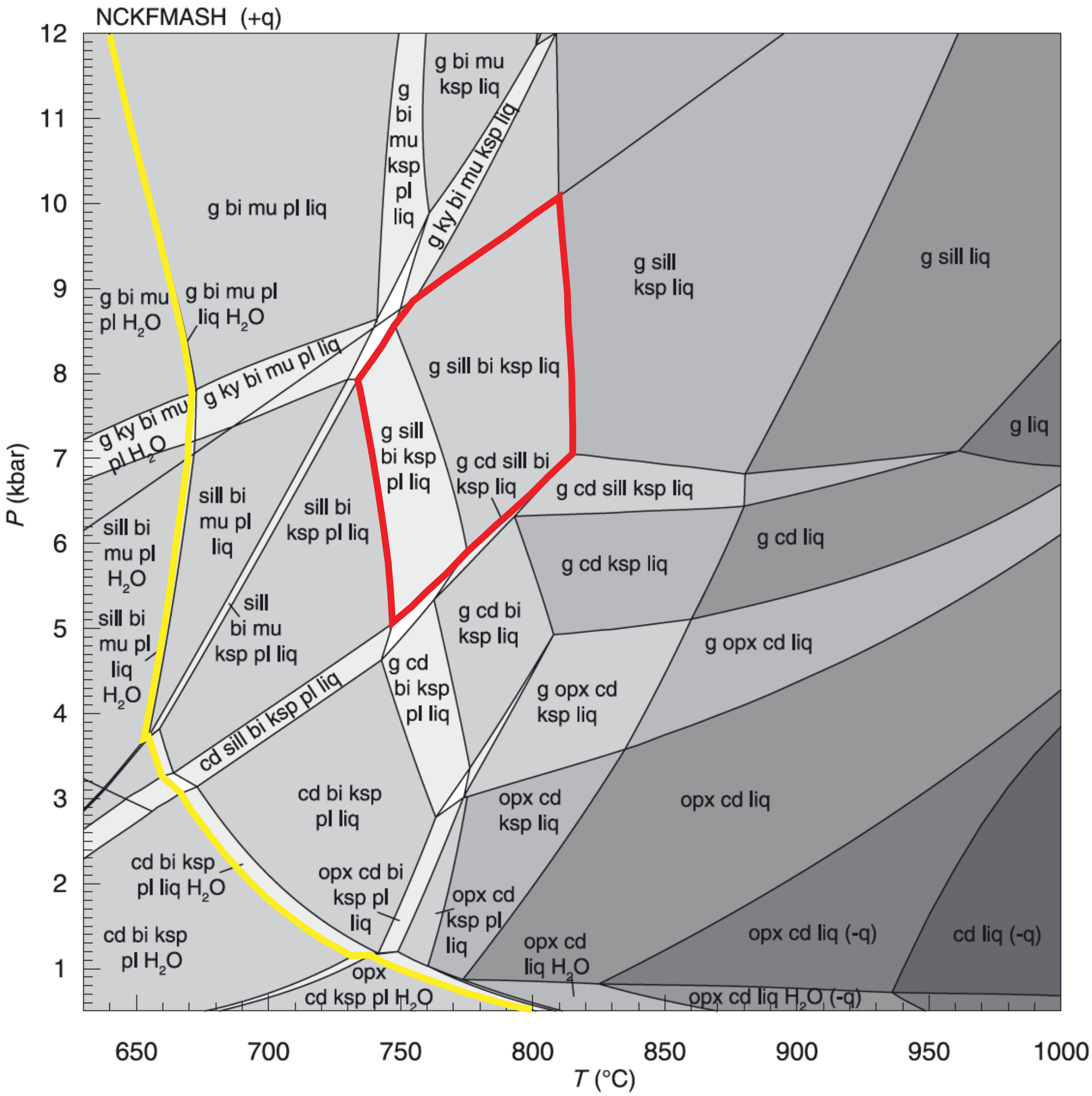

Fig. 4

DOI: https://doi.org/10.2138/am-2019-6906

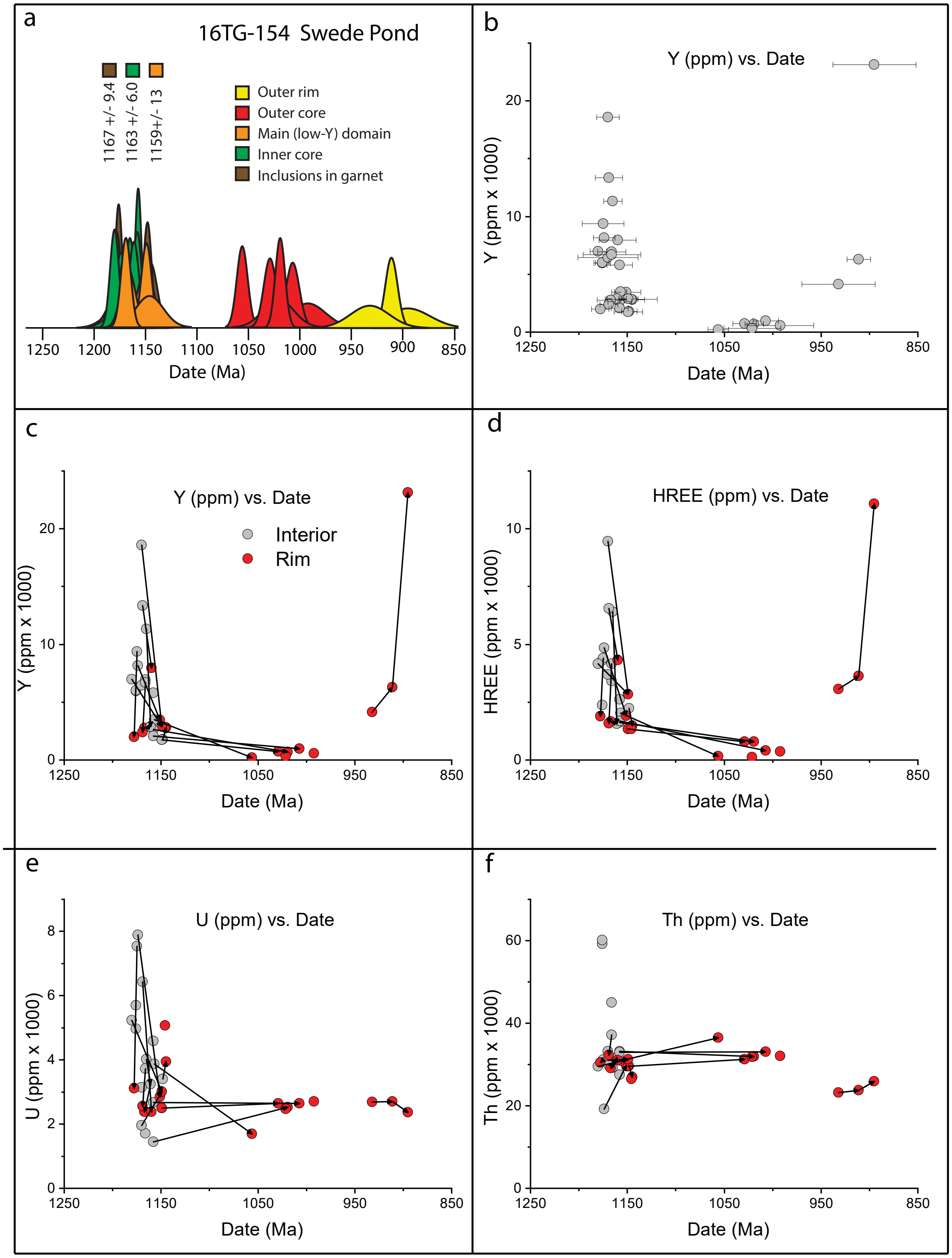

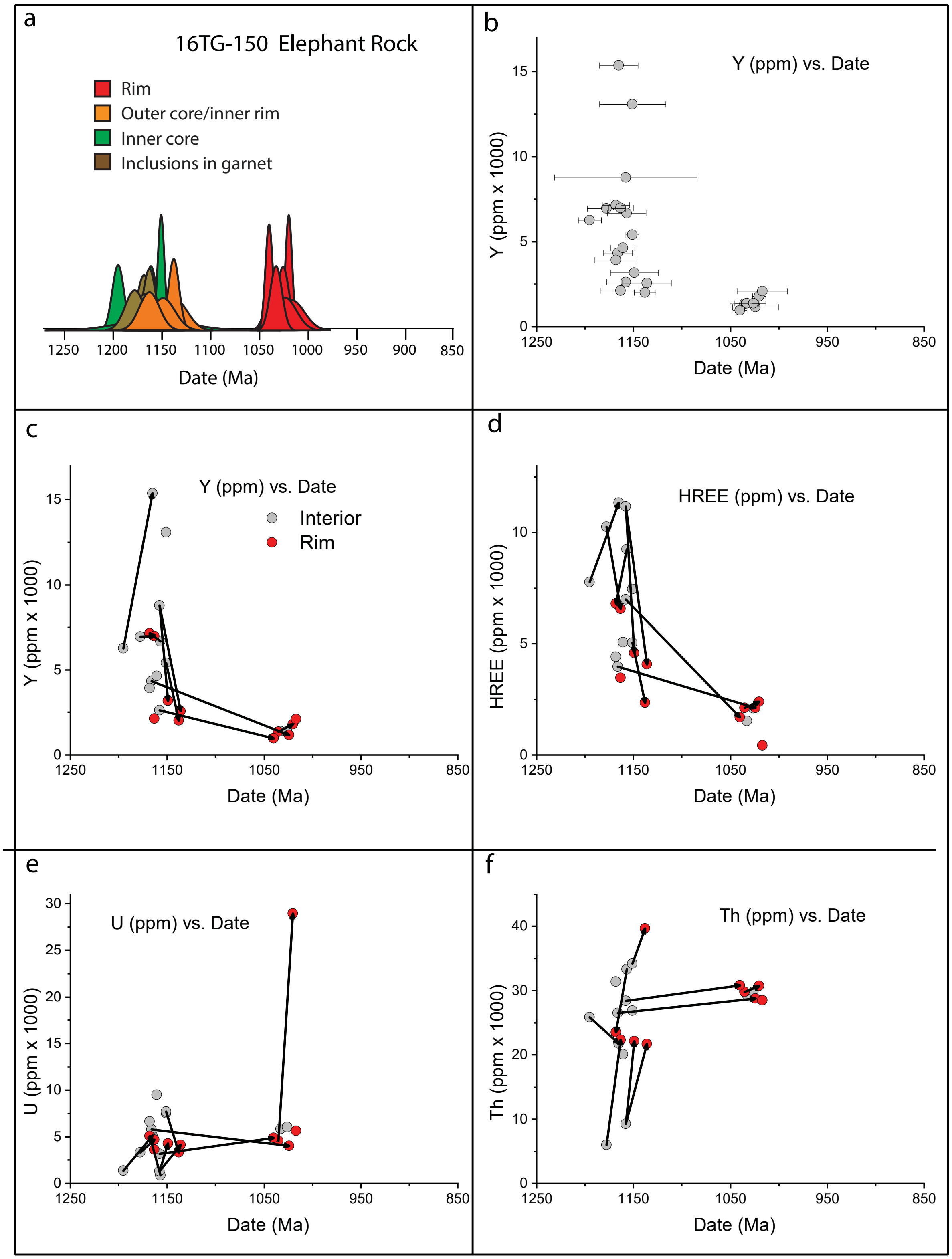
a
16TG-150 Elephant Rock
Rim
Outer core/inner rim
Inner core
Inclusions in garnet
Date (Ma)
b
Y (ppm) vs. Date
Y (ppm x 1000)
Date (Ma)
c
Y (ppm) vs. Date
Interior
Rim
Y (ppm x 1000)
Date (Ma)
d
HREE (ppm) vs. Date
HREE (ppm x 1000)
Date (Ma)
e
U (ppm) vs. Date
U (ppm x 1000)
Date (Ma)
f
Th (ppm) vs. Date
Th (ppm x 1000)
Date (Ma)

DOI: https://doi.org/10.2138/am-2019-6906

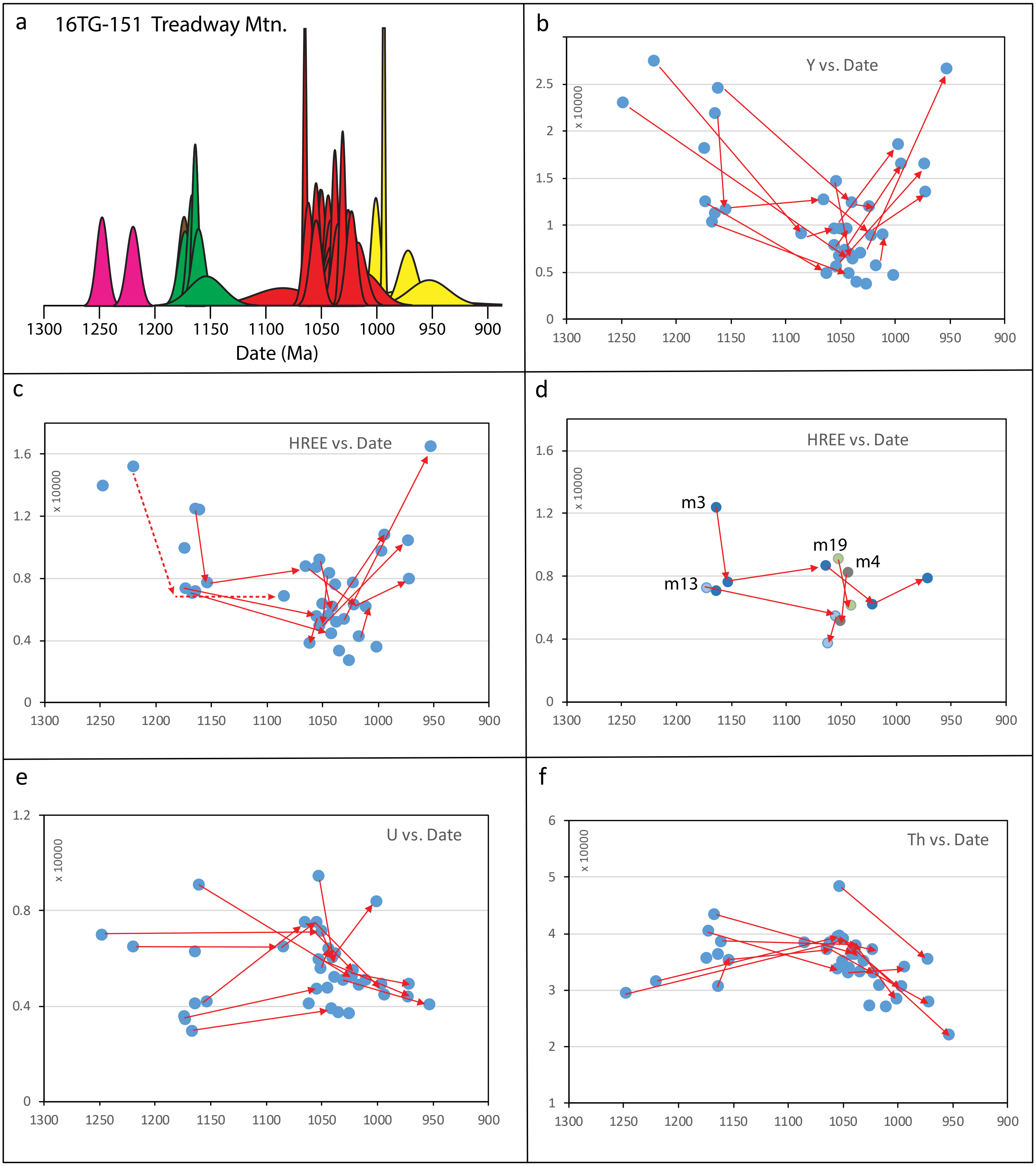

Fig. 6

DOI: https://doi.org/10.2138/am-2019-6906

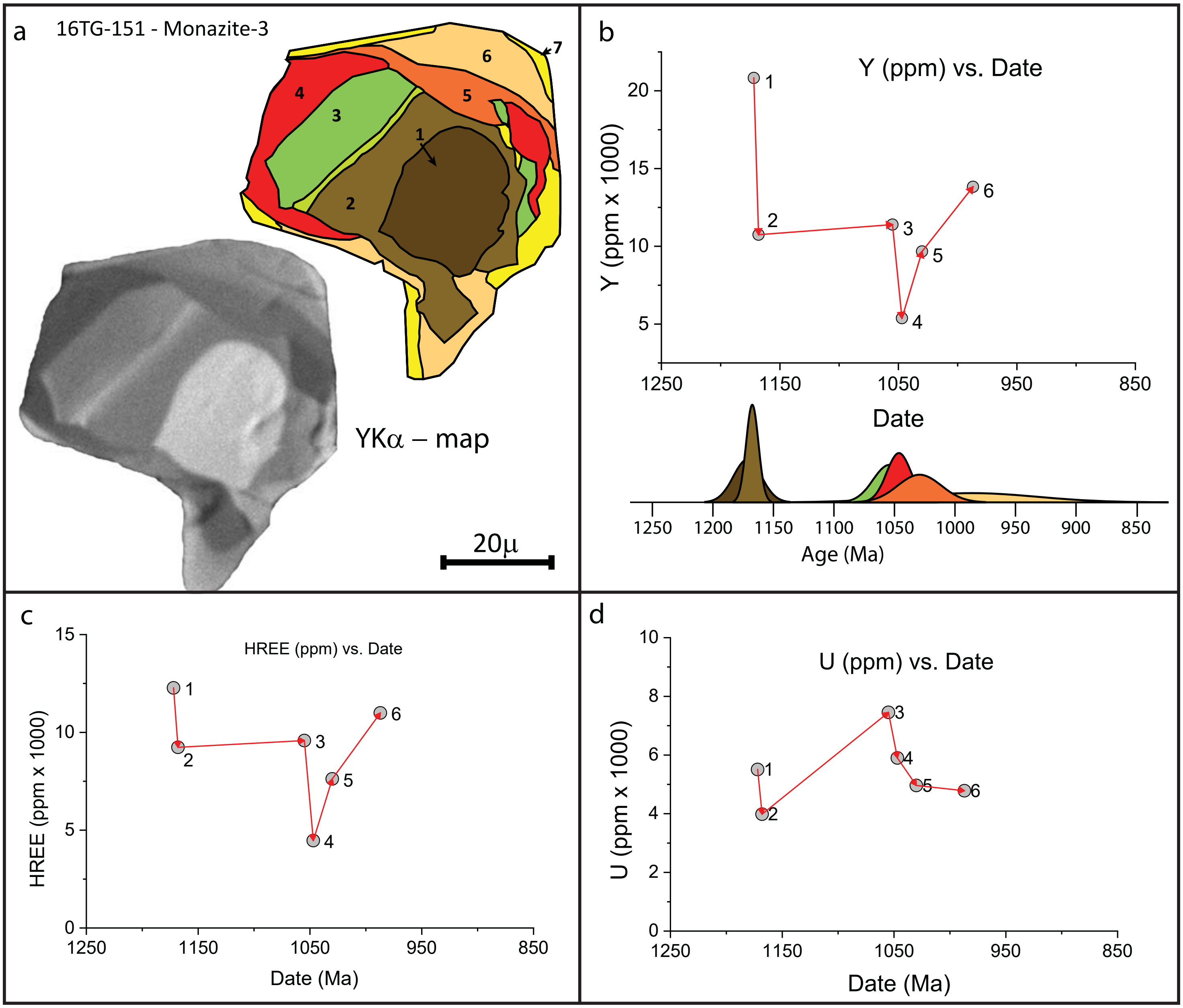

Fig. 8a

DOI: https://doi.org/10.2138/am-2019-6906

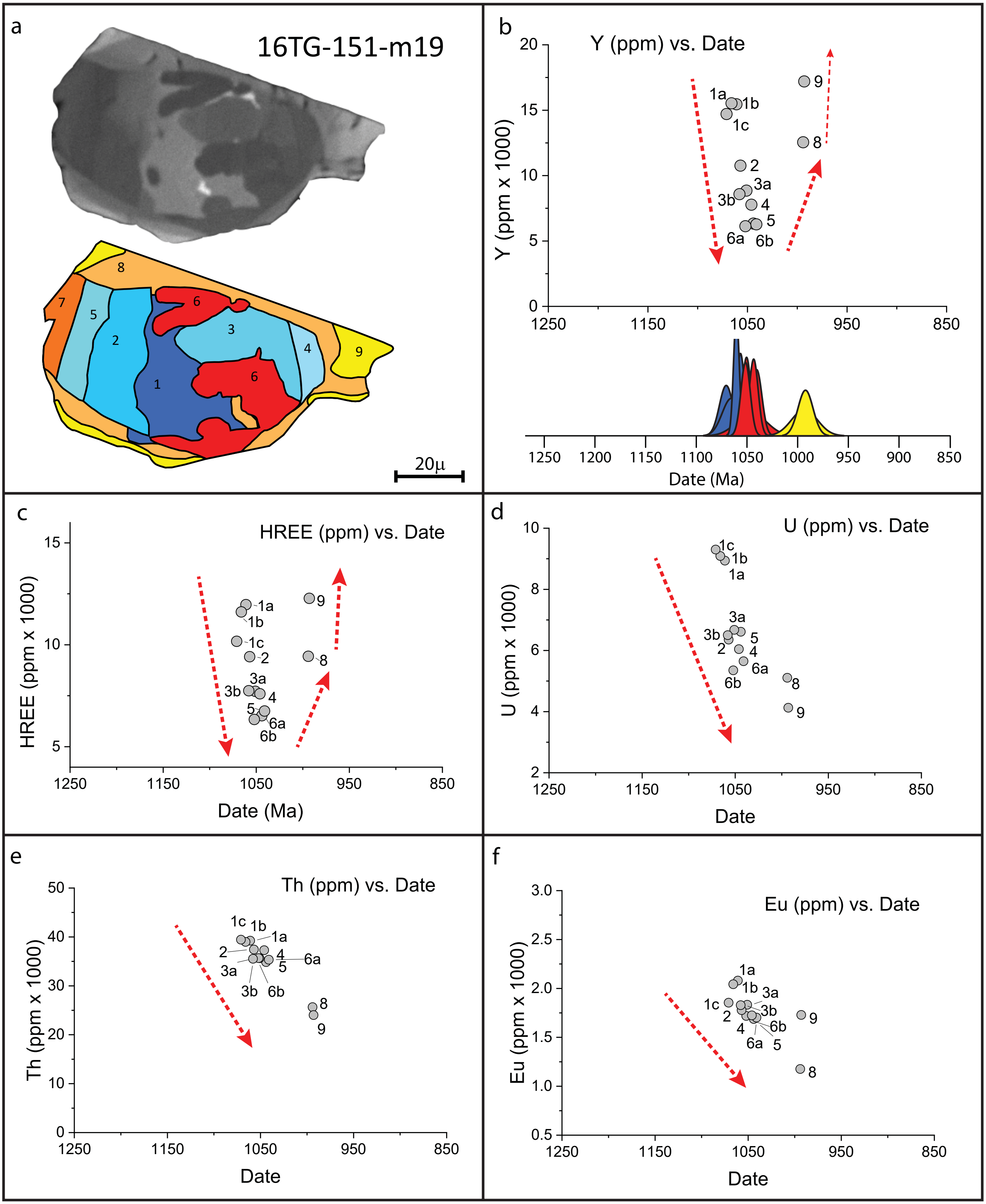

Fig. 8b

DOI: https://doi.org/10.2138/am-2019-6906

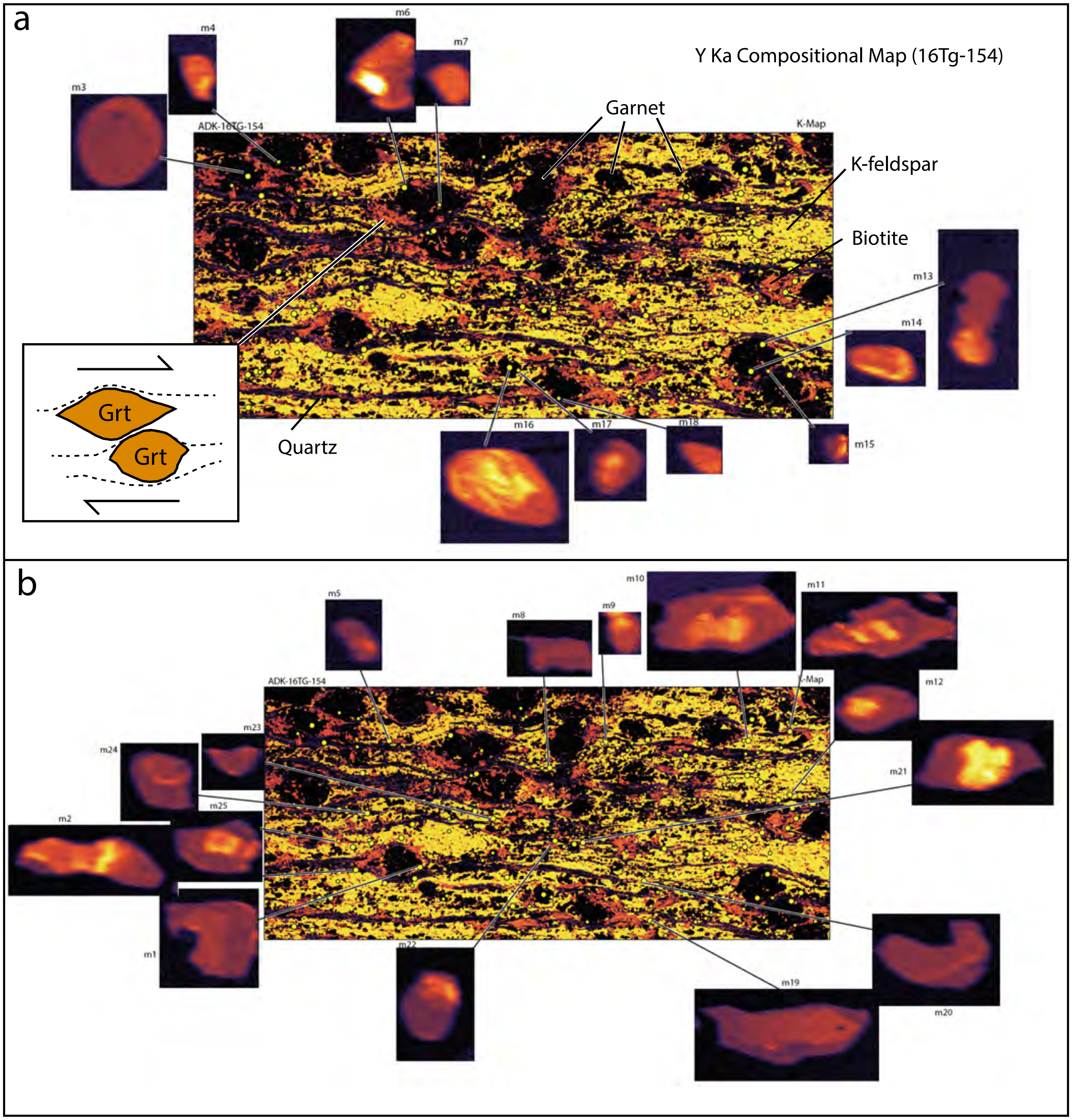

Fig. 9